**Review**

# Strong metal-support interaction of Pt-based electrocatalysts with transition metal oxides/nitrides/carbides for oxygen reduction reaction

**Min Chen, Peng Rao, Zhengpei Miao, Junming Luo, Jing Li, Peilin Deng, Wei Huang, Xinlong Tian**

State Key Laboratory of Marine Resource Utilization in South China Sea, Hainan Provincial Key Lab of Fine Chemistry, School of Chemical Engineering and Technology, Hainan University, Haikou 570228, Hainan, China.

**Correspondence to:** Prof. Zhengpei Miao, State Key Laboratory of Marine Resource Utilization in South China Sea, Hainan Provincial Key Lab of Fine Chemistry, School of Chemical Engineering and Technology, Hainan University, Haikou 570228, Hainan, China. E-mail: zpmiao92@hainanu.edu.cn; Prof. Xinlong Tian, State Key Laboratory of Marine Resource Utilization in South China Sea, Hainan Provincial Key Lab of Fine Chemistry, School of Chemical Engineering and Technology, Hainan University, Haikou 570228, Hainan, China. E-mail: tianxl@hainanu.edu.cn

## Abstract

The practical application of carbon-supported Pt-based catalysts for the oxygen reduction reaction (ORR) in proton exchange membrane fuel cells (PEMFCs) still faces many limitations, including carbon corrosion and their weak interaction with Pt-based nanoparticles (NPs). Harnessing the strong metal-support interaction (SMSI) effects at the interface between Pt-based nanoparticles and alternative corrosion-resistant non-carbon support is an effective strategy to address these issues. The rational design of Pt-based catalysts with favorable SMSI and elucidation of the mechanisms underlying such interactions is indispensable for achieving desirable activity and stability. In this review, first, the basic principles of the ORR are briefly introduced. Next, the formation process of SMSI, construction strategies, and the advantages and drawbacks of representative supports, including transition metal oxides, nitrides, and carbides (TMOs, TMCs, and TMNs, respectively), are fully discussed. Finally, the challenges and prospects in promoting the practical applications of the SMSI effect for ORR are highlighted.

## INTRODUCTION

The accelerated global population growth and massive consumption of fossil fuel energy have induced imbalanced energy shortages and severe environmental disruption. Thus, the development of environment-friendly and sustainable energy technologies has attracted widespread attention to mitigate these phenomena[1-3]. Benefiting from their high energy density and zero carbon emissions, proton exchange membrane fuel cells (PEMFCs) have been considered as one of the most promising energy conversion technologies in residential applications, automobile transportation, and other stationary power systems[4-6]. However, the sluggish kinetics of the cathodic oxygen reduction reaction (ORR) is the major barrier to the further scale-up of PEMFC for large-scale commercialization[7-9]. Carbon-supported Pt nanoparticles (Pt/C) have been widely employed as the ORR electrocatalysts, while the weak interaction between Pt and carbon frequently causes the aggregation, dissolution, Ostwald ripening/coalescence, or detachment of Pt from the carbon support, thus deteriorating the ORR activity and stability[10,11]. Furthermore, carbon supports tend to experience severe corrosion, especially under the high potential encountered during the start-up or shut-down stages. The strong acidic environment (pH < 1) also contributes to catalyst inactivation and short lifetime[8,12], which is a non-negligible factor.

To overcome such shortcomings of carbon support, different types of alternative supports have been exploited to improve the stability of Pt-based catalysts towards ORR in highly oxidative and acidic environments, including graphitic carbon nitride (g-$C_3N_4$), transition metal oxides, carbides and nitrides (TMOs, TMCs, and TMNs, respectively), 2D metal-organic frameworks (MOFs), covalent-organic framework (COFs), layered double hydroxide (LDH), and so on[13-22]. Among them, TMOs, TMNs, and TMCs are considered to be the most promising alternative supports due to their superior corrosion resistance and strong metal-support interaction (SMSI) with Pt nanoparticles (NPs). The driving force of SMSI is defined as minimizing the surface energy of Pt NPs by covering the mobile support suboxides, which provide a variety of possibilities to modulate the catalytic activity, selectivity, and stability of the active species, opening up opportunities for developing highly active and stable ORR catalysts. To be specific, the SMSI of Pt-support usually involves interfacial electron transfer/donation and structural reconstruction at the metal-support interface (defined as electronic and geometric effects), which has the capacity to alter the adsorption energies of the reactants and reaction intermediates at the catalytic active sites situated on the catalyst surface, thereby affecting the activity and stability of catalysts[23,24]. In addition, SMSI is usually accompanied by the encapsulation of supported metal particles by the support, which effectively stabilizes the metal particles, thus improving the stability of the catalyst. Recently, several review articles have shed much new light on SMSI, which provides an effective method to design catalysts with high activity and durability. For example, Wang *et al.* summarized several new routes to construct SMSI involving reductive/oxidative induced SMSI, adsorbate-mediated SMSI (A-SMSI), and wet-chemistry SMSI (wcSMSI) to improve the sinter resistance and catalytic performances of the supported metal catalysts[25]. Luo *et al.* provided an overview of the developments of SMSI and covered its applicability in both thermocatalysis and electrocatalysis systems[26]. Pu *et al.* reviewed various spectroscopic and microscopic techniques capable of characterizing the SMSI phenomena and systematically explored the effect of SMSI on catalytic activity/selectivity[27]. However, these SMSI analyses were largely limited to catalytic reactions involving CO, $CH_4$, $CO_2$, or methanol as the main reactant, lacking relevant summaries and mechanistic elucidation in the field of ORR.

In this review, particular attention is paid to the recent progress in the design, construction, and emerging applications of SMSI in ORR catalysts. Particularly, we start by optimizing the intrinsic activity of TMOs, TMNs, and TMCs supports. By elaborately selecting their compositions, precisely modulating the synthesis methods, and further adjusting the metal-support interaction, we aim to improve the ORR activity and stability of the catalysts. This distinguishes our view from the previous review articles[27,28]. Firstly, the basic principles of the ORR, some descriptors of the computational activity, and electrochemical activity are briefly introduced. Secondly, detailed strategies of manipulating SMSI through rational design of catalyst structures and different atmosphere treatments in recent years are summarized. In addition, the precise synthetic methods and effective improvement strategies of several TMO-, TMN-, and TMC-supported Pt-based catalysts applications for ORR are discussed. Finally, the prospects and challenges of SMSI for ORR catalysts are provided.

## BASIC PRINCIPLES OF THE ORR
### Mechanisms of the ORR
The ORR process generally consists of four steps as follows: (1) diffusion and adsorption of $O_2$ on the electrocatalyst surface; (2) electron migration from the electrode to adsorbed $O_2$ molecules; (3) weakening and splitting of O=O bonds; and (4) removal of the generated species to the electrolyte[29]. Typically, $O_2$ can be reduced to $H_2O$ or $H_2O_2$ through two different electron transfer pathways: the direct four-electron transfer pathway (Eq. 1) and the indirect two-electron transfer pathway (Eq. 2). Four-electron transfer occurs to reduce molecular oxygen to water, facilitating the ORR process. However, it is always accompanied by the reduction of the two-electron pathway, resulting in the partial reduction of oxygen to hydrogen peroxide products, which reduces the electrocatalytic selectivity. Both four- and two-electron transfer pathways involve various oxygen-containing intermediates such as *O, *OH, or *OOH (*represents the active catalytic site)[30-32]. More specifically, there are three possible reaction mechanisms: dissociative, associative, and peroxo mechanisms, as shown in Figure 1A. For the dissociative and associative mechanisms of the four-electron transfer pathway, their difference depends on whether they involve the formation of *OOH intermediate[33].

$$O_2 + 4H^+ + 4e^- \rightarrow 2H_2O, E^0 = 1.229 \text{ V } vs. \text{ RHE} \tag{1}$$

$$O_2 + 2H^+ + 2e^- \rightarrow 2H_2O_2, E^0 = 0.695 \text{ V } vs. \text{ RHE} \tag{2}$$

where RHE represents the reversible hydrogen electrode.

### Linear scaling relationships
Density functional theory (DFT) calculations have been extensively used to understand the free energies of those intermediates and further estimate the ORR performance. By extending the calculations to various close-packed metal surfaces, the scaling relationship between ORR activity and oxygen adsorption energy ($\Delta E_o$) have been eventually plotted in "volcano plots" with Pt located at the extreme tip of the linear currently (as shown in Figure 1B)[34]. Generally, the $\Delta E_o$ of Pt-based catalysts is determined by the position of the *d*-band center relative to the Femi level, while the shift of the *d*-band center can be modulated by alloy with other elements (ligand effect), such as Ni, Co, Fe, *etc.*[33,35]. An ideal candidate metal should have a moderate affinity for oxygen. More specifically, if the metals bind oxygen too strong, the ORR will be retarded due to the difficulty in removing intermediates (O* or OH*) formed by proton-coupled electron transfer, whereas the metals bind oxygen too weak, the $O_2$ adsorption and later dissociation to form O* will be constrained. Additionally, a series of catalysts with the SMSI effect, compared to PtM/C catalysts, can rapidly accelerate the electron transfer in the metal-support interface and precisely regulate the *d*-band
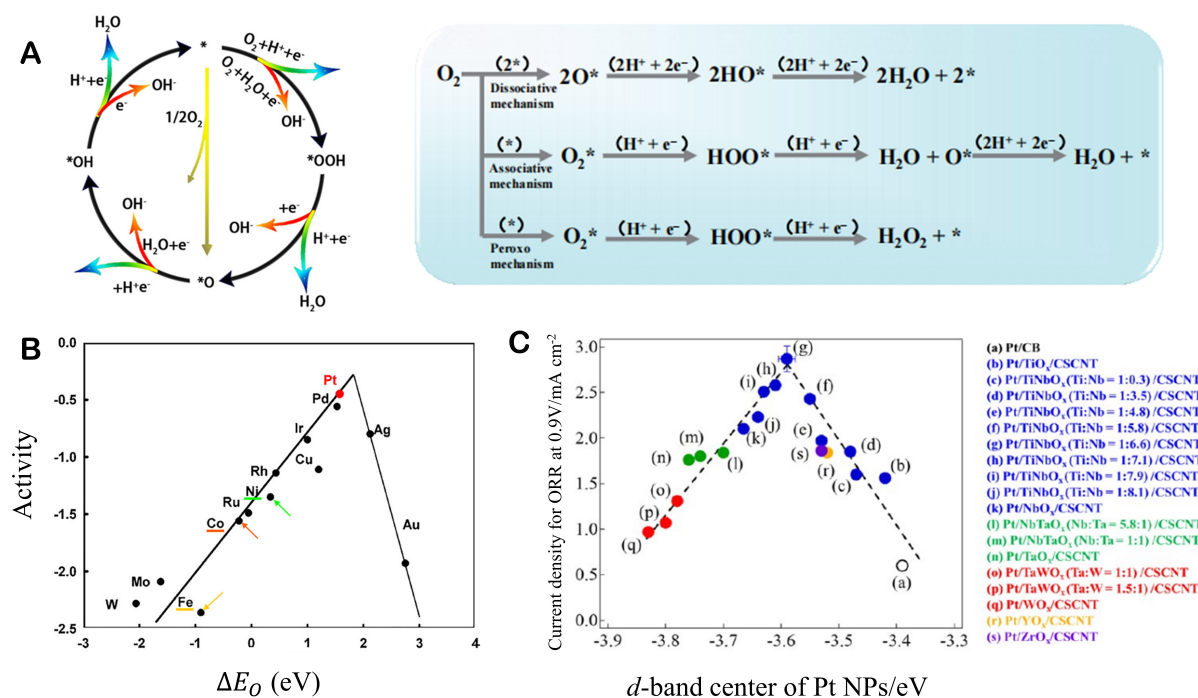
**Figure 1.** (A) ORR mechanism in acidic (blue line) and alkaline (red line) electrolytes and proposed pathways for ORR. Reproduced with the permission of Ref.[31] Copyright 2021, Elsevier. (B) Trends in oxygen reduction activity plotted as a function of the oxygen binding energy. Reproduced with permission of Ref.[34] Copyright 2004, American Chemical Society. (C) Relationship between the *d*-band center of Pt and the current density at 0.9 V (*vs.* RHE) for the ORR. The Pt NPs were deposited on support materials (a)-(s) shown on the right. Reproduced with the permission of Ref.[36] Copyright 2021, American Chemical Society.

center of the catalyst. Inspired by this, Ando *et al.* constructed a similar "volcano-type" of a series of binary transition metal oxides/cup-stacked carbon nanotubes supported Pt NPs (Pt/$M_1M_2O_x$/CSCNTs) catalysts to demonstrate that the *d*-band center values of Pt/$M_1M_2O_x$/CSCNTs catalysts can be downshift in a controlled manner by reasonable selection and precise regulation of $M_1$ and $M_2$ in the $M_1M_2O_x$/CSCNTs support (as shown in Figure 1C)[36]. The Pt/$TiNbO_x$ (Ti/Nb = 1:6.6 in atomic ratio)/CSCNTs catalysts with ca. 0.2 eV downshift of the *d*-band center from that of Pt exhibited the maximum ORR activity and stability, resulting from the ligand effect in the metal-support structure and the SMSI effect as well.

## METHODS TO INDUCE THE STRONG METAL-SUPPORT INTERACTIONS

With the rapid development in the field of SMSI, the methods to induce SMSI have also been continuously developed and evolved for improving the sinter resistance and catalytic performance of the supported metal catalysts. To date, several SMSIs construction strategies, including SMSI, oxidative strong metal-support interaction (O-SMSI), A-SMSI, wcSMSI, reaction-induced SMSI (R-SMSI), and laser-induced SMSI (L-SMSI) have been reported with different construction conditions[26], such as reduction, oxidation, adsorbates, photo-treatment, *etc.* Tuning the SMSI behaviors has also been proven to be one of the most efficient methods for manipulating catalytic performance. Here, we briefly summarize the recent progress in SMSI, focusing on different methods for constructing SMSI and their advantages and disadvantages. The timeline for different types of SMSI is shown in Figure 2.

### Strong metal-support interaction (SMSI)

Since the first report[37] and follow-up work[38] in the late 1970s by Tauster *et al.*, the classical strong metal-support interaction (SMSI), a term coined to describe a phenomenon that the loss of small molecules (such
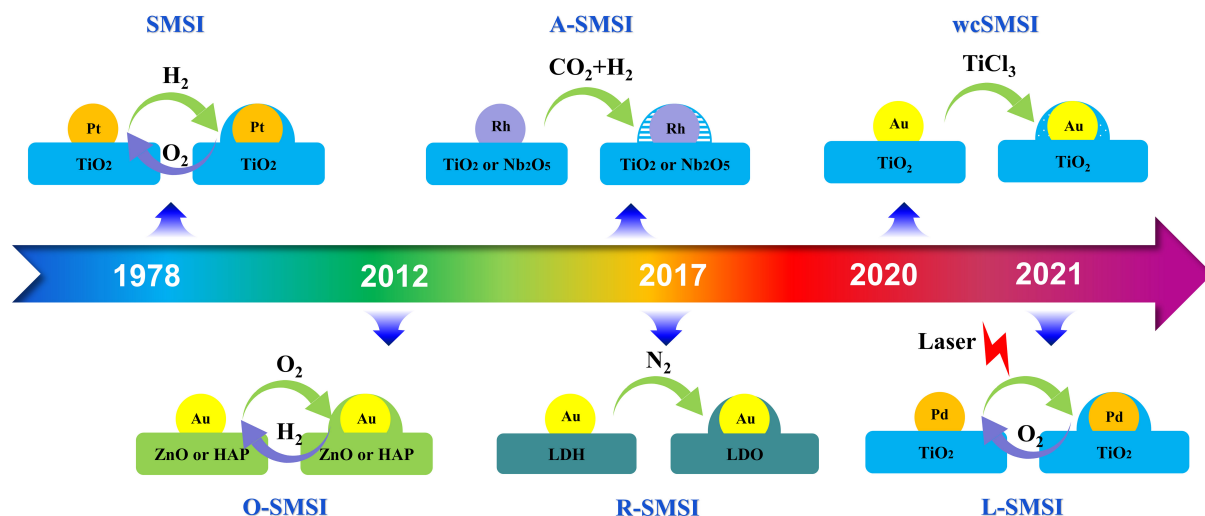
**Figure 2.** A timeline of representative achievements in the field of SMSI.

as CO and $H_2$) chemisorption of titania-supported platinum group metals (PGMs) after high-temperature reduction (HTR) with hydrogen (as shown in Figure 3A), has garnered a great deal of interest and attention in the field of heterogeneous catalysis. Initially, the inhibition of chemisorption was assigned to the electron perturbation of the system, i.e., the intermetallic bonding between PGMs and Ti cations under hydrogen atmospheres[10]. Subsequently, an increasing number of studies have shown that the primary reason for the CO adsorption suppression is the partially reduced layer of $TiO_2$ encapsulating its supported PGMs, thereby obscuring the metal surface adsorption sites[10,39-41]. With the application of high-resolution real-space methods, the primary characteristics of SMSI have been revealed successively and eventually identified by four criteria, including: (1) remarkable suppression of the chemisorption of small molecules on the metal; (2) mass transport induced by metal NPs encapsulated by the reduced support; (3) electron transfer from the support to metal NPs; and (4) a reversal of the above phenomena on reoxidation[25,42]. The electronic/ geometric effects and synergistic interactions between metal and support arising from these features endow the catalysts with great tunability and stability for their structure and properties[43,44]. However, metals with high surface energy and large work functions are believed to be indispensable for the formation of SMSI, that is, a series of low work function and surface energy IB group metals NPs, such as Au, Cu, and Ag, fail to manifest SMSI behaviors on $TiO_2$, as shown in Figure 3B[45-48]. Additionally, the SMSI effect is limited existing on reducible oxide supports, which inevitably influences the catalyst performance owing to the low electrical conductivity. Furthermore, the traditional method for inducing SMSI requires a high-temperature reduction in the $H_2$ atmosphere to activate the surface of reducible metal oxide support, which usually causes the aggregation of metal NPs before forming the barriers under harsh reduction conditions, in turn affecting the catalytic performance. Therefore, it is necessary to develop several new routes for constructing SMSI to elucidate its universality in catalytic systems.

**Oxidative strong metal-support interaction (O-SMSI)**

O-SMSI, a novel strategy to construct SMSI by high-temperature oxidative treatment, was first reported by Liu *et al.* in an Au/ZnO-nanorod catalyst[49]. The reversible encapsulation of Au NPs by a thin layer of zinc oxide and reduction of small-molecule adsorption are identical to the traditional SMSI except that the electron transfer of O-SMSI is from Au NPs to support. This new discovery not only broadens the occurrence of SMSI but also points to new directions in the study of SMSI for Au-based catalysts. Subsequently, a series of studies extended the support of SMSI from oxide to non-oxide systems such as
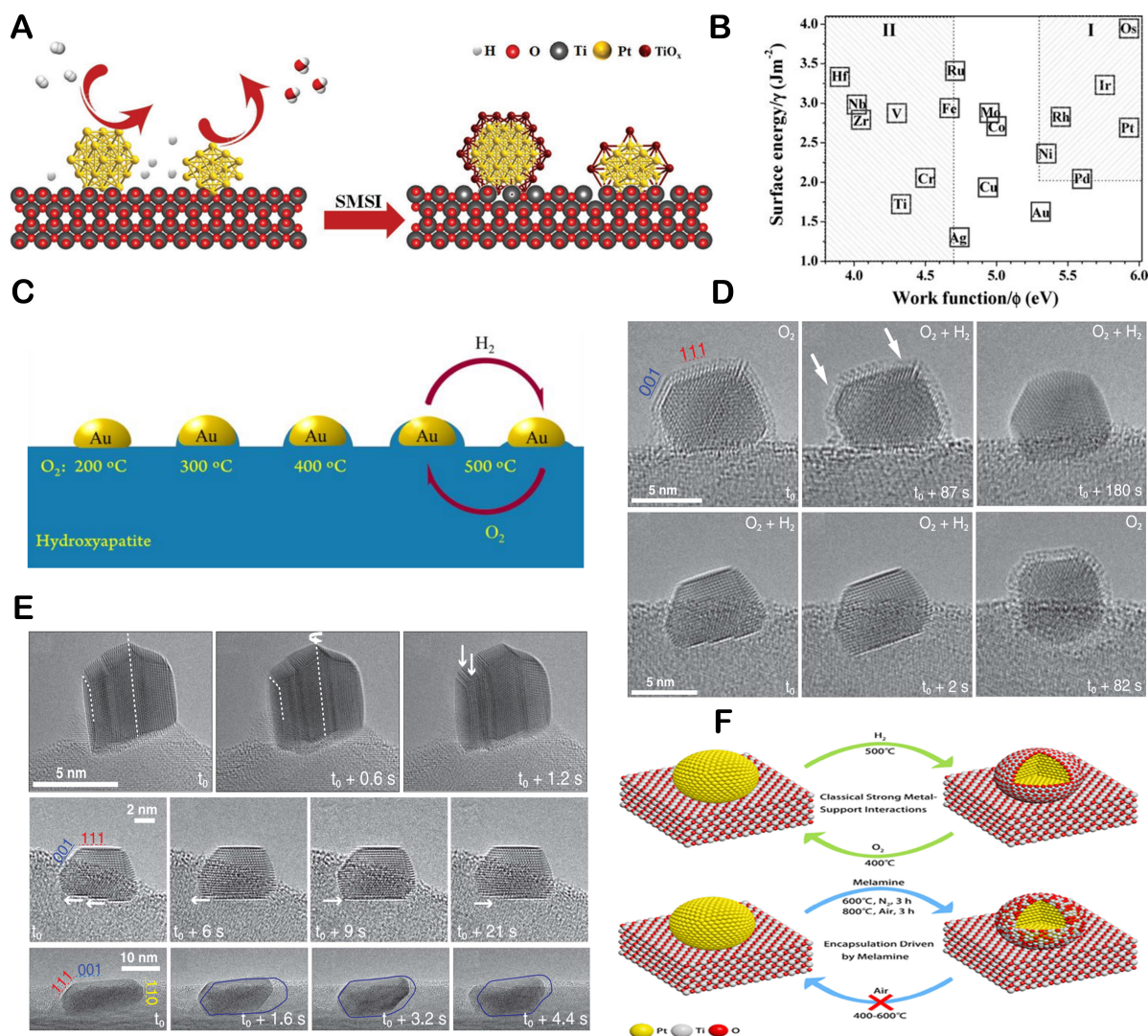
**Figure 3.** (A) Schematic illustrations of the formation process of SMSI in Pt/TiO$_2$. Reproduced with the permission of Ref.[26] Copyright 2022, John Wiley and Sons. (B) Relationship between surface energy ($\gamma_M$) and work function ($\varphi$) of different transition metals. Reproduced with the permission of Ref.[48] Copyright 2005, American Chemical Society. (C) Schematic illustrations of the formation process of O-SMSI in Au/HAP. Reproduced with the permission of Ref.[50] Copyright 2016, American Chemical Society. HRTEM images of (D) The destabilization of overlayer and (E) the dynamic behavior of Pt NPs on the support interface. Reproduced with the permission of Ref.[10] Copyright 2022, Science. (F) Different encapsulation functions between O-SMSI and classical SMSI in Pt/TiO$_x$. Reproduced with the permission of Ref.[53] Copyright 2021, American Chemical Society.

hydroxyapatite (HAP) (as shown in Figure 3C), opening a new avenue for the design of highly stable supported gold catalysts[50,51]. With the diversification of measurement methodologies and the advancement of characterization techniques, the atomic-level structural evolution of TiO$_2$ encapsulated layer in a redox-active regime (O$_2$ + H$_2$ atmosphere) and the dynamic behavior of particles and interfaces induced by metal-support interaction were systematically revealed via *in situ* transmission microscopy by Frey *et al.*[10]. With the atmosphere switches from O$_2$ to a redox-active H$_2$-O$_2$ mixture, the TiO$_2$ encapsulation layer was completely retracted from all the particles (as shown in Figure 3D), and the particles exhibited dynamic behavior on the support interface and ceased as soon as H$_2$ was completely removed from the reactor cell (as shown in Figure 3E), whereby the overlayer is also reformed around the NPs. This phenomenon indicates that the encapsulation layer induced by the O-SMSI and SMSI strategy is vulnerable to the external

environment (e.g., humid atmosphere), resulting in encapsulation failure, metal agglomeration, and a dramatic decrease in stability. To optimize the stability of the $TiO_2$ overlayers, Liu *et al.* reported that $Au/TiO_2$ catalysts modified with melamine and annealed at 600 °C in $N_2$ atmosphere and further treatment at 600 °C in air atmosphere to form an amorphous and permeable $TiO_x$ encapsulation layer on Pt NPs, which is extremely stabilized against re-oxidize in air, in stark contrast to the retreat of the $TiO_x$ encapsulation layer by later oxidation treatment in previous SMSI (as shown in Figure 3F)[52]. Subsequently, they expanded this strategy to $TiO_2$-supported Pd and Rh NPs, a promising way for designing supported platinum group metal-based catalysts with high activity and stability[53].

### Adsorbate-mediated SMSI (A-SMSI)

Notably, the aforementioned examples of SMSI and O-SMSI typically rely on high-temperature thermal treatment (≥ 500 °C) while inevitably decreasing the catalytic performance due to blockage of metal active sites. Matsubu *et al.* reported an adsorbate-mediated SMSI (A-SMSI) encapsulated strategy that forms with the treatment of $TiO_2$- and $Nb_2O_5$-supported Rh NPs in $20CO_2$:$2H_2$ atmosphere at a relatively low temperature (150-300 °C)[54]. *In situ* spectroscopy and microscopy demonstrated that the thickness of the A-SMSI overlayer is almost twice that of the SMSI overlayer, thanks to the adsorbates $HCO_x$ species strongly bounded on the support to induct the formation of oxygen-vacancy, prompting the migration of $HCO_x$-functionalized support onto the metal to form an extremely stabilized encapsulated state against re-oxidation by the air atmosphere (As shown in Figure 4A, line a-b-c). Later, the A-SMSI strategy was labeled as "low-temperature induction" and "encapsulation stability" with its extended application to $Cu/CeO_2$[55] and $Ru/MoO_3$[56]. Nowadays, the induction of A-SMSI overlayer is not restricted to $CO_2$-$H_2$ atmospheres only. For example, Li *et al.* successfully constructed A-SMSI on a commercial $Cu/ZnO/Al_2O_3$ catalyst under $H_2/H_2O/CH_3OH/N_2$ mixture atmosphere at 300 °C (as shown in Figure 4B) and found that the $ZnO_x$ species migrated onto the surface of metallic $Cu^0$ NPs to constitute a stable encapsulated structure, and the proper degree of encapsulation could be achieved by adjusting the exposure time[57]. Combined with DFT calculations, the improved methanol steam reforming reaction activity of $Cu/ZnO/Al_2O_3$ catalysts was attributed to the increased number of the $ZnO_x$-Cu interfacial sites (as shown in Figure 4C).

### Wet-chemistry SMSI (wcSMSI)

Besides the A-SMSI strategy enables encapsulation at relatively low temperatures, the wcSMSI method is another effective strategy for achieving SMSI in an aqueous solution at room temperature, which not only avoids the conventional high-temperature redox condition causing pre-sintered metal NPs but also effectively stabilizes the metal NPs against re-oxidation. As an example, an $Au/TiO_2$-wcSMSI catalyst synthesis was reported by Zhang *et al.* that the average diameter of the $TiO_2$ overlay was 2 nm, and the supported Au NPs were completely encapsulated[58]. In addition, they provide a proof-of-concept design to reveal the mechanisms of enhancing the catalytic activity of $Au_{55}$ cluster on inert $SiO_2$ support covered by $TiO_x$ overlayers ($Au_{55}@Ti/SiO_2$) through DFT calculations (as shown in Figure 4D), thereby extending the wet-chemistry method to inert oxide supported field. Recently, Hao *et al.* synthesized a $Pt@TiO_x/TiO_2$ catalyst via the wcSMSI strategy, which consists of Pt NPs decorated by amorphous $TiO_x$ overlayers and exhibits extremely active and stable in $C_3H_8$ and $C_3H_6$ combustion compared with the conventional supported $Pt/TiO_2$ catalyst owing to the electronic interaction between Pt and $TiO_x$ ($Pt^{x+}/Pt^0 \leftrightarrow Ti^{3+}/Ti^{4+}$)[59]. Since the wcSMSI process protects the severe sintering of the NPs from the high temperature, the stability of catalysts is also substantially ensured.

### Reaction-induced SMSI (R-SMSI)

In particular, the abovementioned types of SMSI constructions predominantly rely on the redox oxide supports, such as $TiO_2$, ZnO, $Nb_2O_5$, *etc.* However, the relatively redox-inert supports (e.g., Mg- and Al-based oxide supports) are unsuitable for the construction of SMSI as their surface activation is challenging.
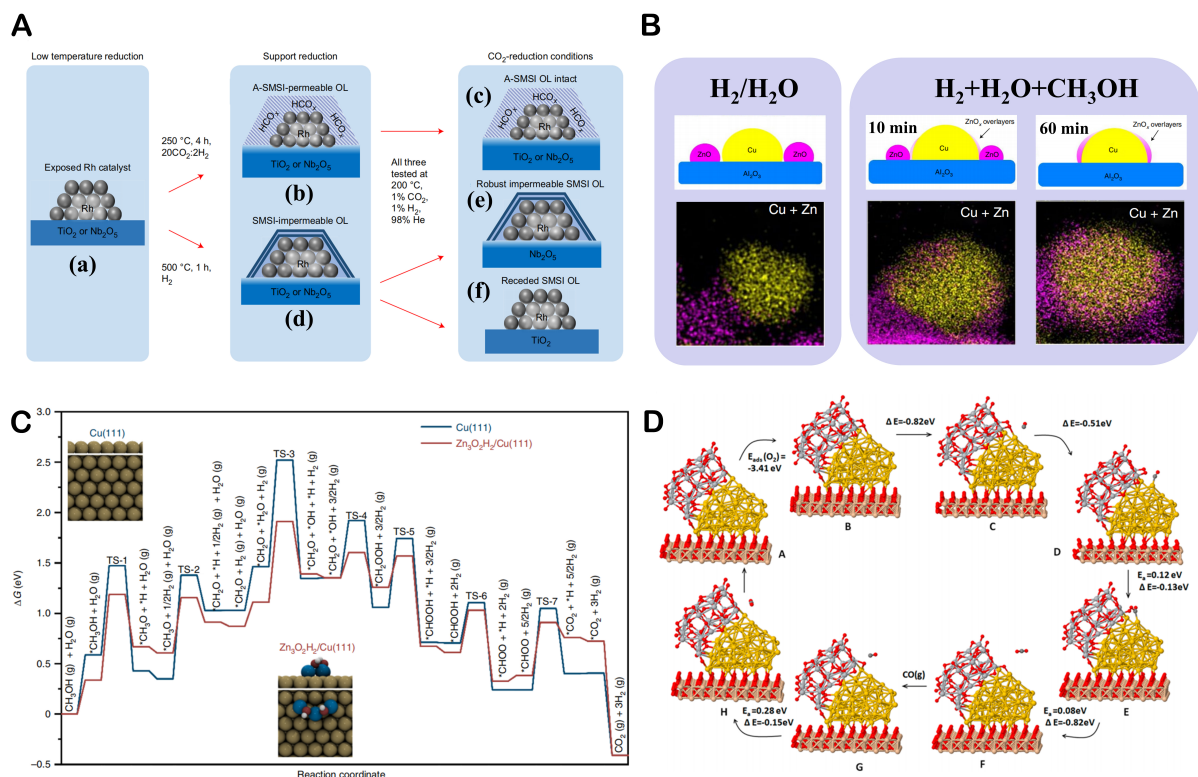
**Figure 4.** (A) A-SMSI and Classical SMSI overlayer structure and behavior. Reproduced with the permission of Ref.[54]. Copyright 2017, Springer Nature. (B) Structural change of $Cu/ZnO/Al_2O_3$ catalyst after different pretreatments and the corresponding elemental distribution from transmission electron spectroscopy images. The DFT simulations over (C) $Cu/ZnO/Al_2O_3$. Reproduced with the permission of Ref.[57]. Copyright 2022, Springer Nature. (D) $Au_{55}@Ti/SiO_2$ model with two $TiO_x$ atomic layers. Reproduced with the permission of Ref.[58]. Copyright 2019, American Chemical Society.

Reaction-induced SMSI (R-SMSI) strategy is an effective method to induce the activation, migration, and encapsulation of redox-inert support via its phase transition. For example, Wang *et al.* successfully achieved R-SMSI between Au NPs and Mg-Al layered double oxides (LDO) vis a high-temperature treatment in nitrogen atmosphere[60]. The hydroxide-to-oxide support transformation is the prerequisite for the construction of R-SMSI, and if Au NPs were loaded directly onto the LDO surface, the R-SMSI structure was not obtainable under the same conditions (as shown in Figure 5A). Then, Dong *et al.* reported that the cyclic change ($MoC_x$-to-$MoO_3$) in the support of $Au/MoC_x$ catalyst under a 20 vol% $CH_4$/He atmosphere can realize R-SMSI[61]. Later, they demonstrated that R-SMSI can also be achieved in the Ni/BN catalysts under the same conditions due to the BN-to-$BO_x$ interfacial change[62]. In other studies, the support phase change between $BaCO_3$-to-BaO of Co/BaO and $Mn_3O_4$-to-$Mn_2O_3$ of $Pt/Mn_2O_3$ catalysts were both formed R-SMSI and exhibited excellent catalytic activity and stability[15,63]. Recently, a reversible reaction of $MgO+CO_2 \leftrightarrow MgCO_3$ was employed to induce the R-SMSI of Au/MgO catalysts in a flowing $CO_2$ atmosphere (as shown in Figure 5B)[64]. $CO_2$ was applied to react with MgO support, and the $MgCO_3$ was subsequently decomposed into a regenerated MgO overlayer to encapsulate the Au NPs. Intriguingly, the direct application of $MgCO_3$ as a support is also able to realize the $MgCO_3$-to-MgO phase transition and to construct a MgO overlayer on Au NPs. These studies demonstrate that the SMSI effect can also be constructed on relatively redox-inert supports, and the mobility of the support after the phase change is significantly higher than that of the original support, which also implies that the encapsulation rate of metals by the R-SMSI strategy seems to be faster than that of classic SMSI.
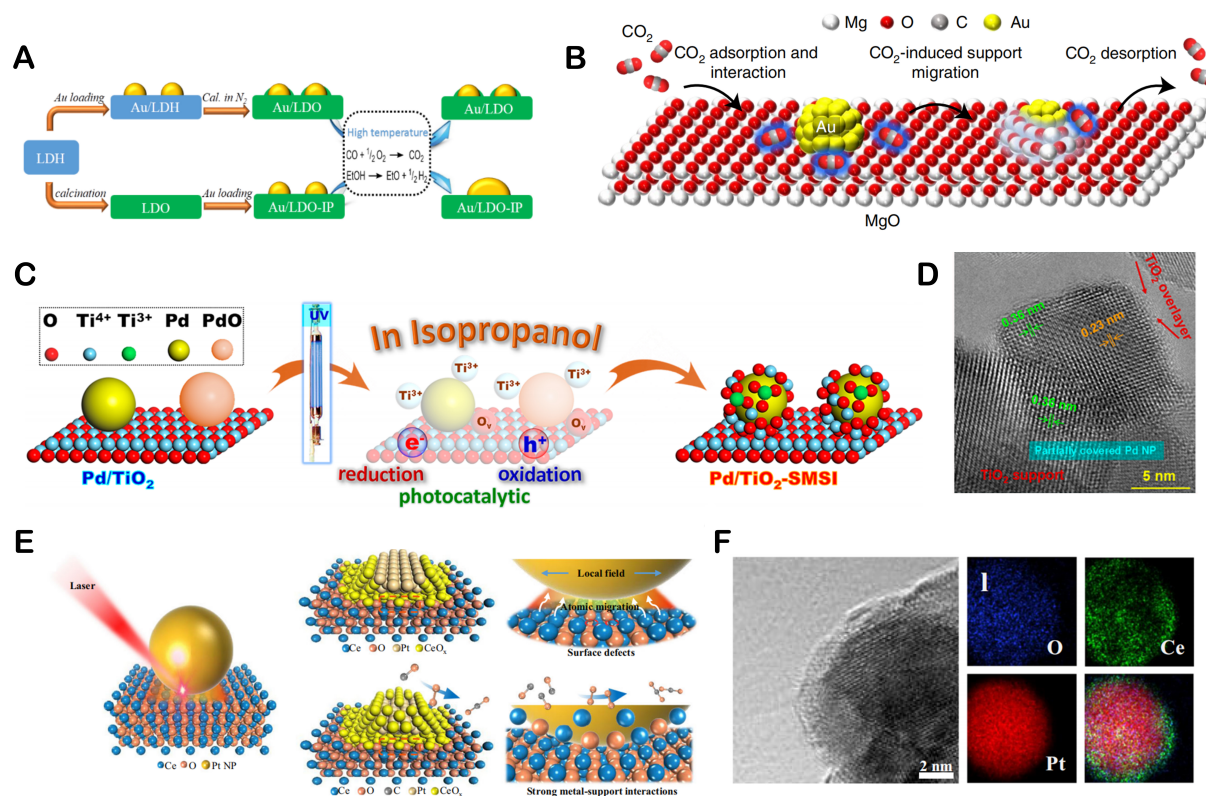
**Figure 5.** Schematic illustrations of the formation process of (A) R-SMSI in Au/LDO. Reproduced with the permission of Ref.[60] Copyright 2017, American Chemical Society, (B) R-SMSI in Au/MgO. Reproduced with the permission of Ref.[64] Copyright 2021, Springer Nature, (C) L-SMSI in Pd/TiO$_2$. (D) TEM images of Pd/TiO$_2$. Reproduced with the permission of Ref.[65] Copyright 2021, American Chemical Society. (E) Schematic illustrations of the formation process of L-SMSI in Pt/CeO$_2$. (F) TEM images of Pt/CeO$_2$. Reproduced with the permission of Ref.[66] Copyright 2021, Springer Nature.

### Laser-induced SMSI (L-SMSI)

Similar to the wcSMSI, L-SMSI also enables the migration of metastable supports to facilitate SMSI formation without specific gaseous atmospheres and thermal treatment. Recently, Chen *et al.* successfully constructed L-SMSI on a Pd/TiO$_2$ catalyst by a photochemistry-driven methodology[65]. Specifically, when excitation energy supplied by ultraviolet (UV) irradiation was greater than the band gap of titanium dioxide (3.1 eV), the separated photoinduced reductive electrons (e$^-$) and oxidative hole (H$^+$) were generated to trigger the formation of Ti$^{3+}$ species/oxygen vacancies (O$_v$) and then interfacial Pd-O$_v$-Ti$^{3+}$ sites, finally constructing the L-SMSI structures (as shown in Figure 5C and D). Subsequently, this as-constructed L-SMSI layer is reversible between retraction on thermal O$_2$ treatment and re-encapsulation on UV irradiation. Similarly, the L-SMSI strategy has been extended to CeO$_2$-supported Pt system catalysts and even to non-reducible oxide supports such as Al$_2$O$_3$ and MgO. Zhang *et al.* applied an ultrafast laser to a Pt/CeO$_2$ catalyst to boost the formation of surface defects and the migration of metastable CeO$_x$, and succeeded in creating porous overlayers of CeO$_x$ on Pt NPs (as shown in Figure 5E and F), which exhibit superior catalytic activity and stability[66].

In summary, we briefly reviewed some typical strategies for constructing SMSI on various atmospheric conditions, annealing temperatures, and oxide and non-oxide supports (as shown in Table 1). These new types displayed similar properties to classical SMSI, including the electron and mass transfer between metal NPs and substrates, the encapsulation of metal species by the migrating substrate, and the suppression of the adsorption behavior of small molecules. Furthermore, they also exhibited remarkable strengths over

**Table 1. Comparison between SMSI and novel construction strategies**

|  | SMSI | O-SMSI | A-SMSI | wcSMSI | R-SMSI | L-SMSI |
|---|---|---|---|---|---|---|
| Metal | VIII group metals | VIII/IB group metals | VIII/IB group metals | VIII/IB group metals | VIII/IB group metals | VIII group metals |
| Support | Reducible metal oxide | Hydroxyapatite, phosphate, and ZnO | Reducible metal oxide | $TiO_2$ | LDO, $MoO_3$, MgO, BaO, $Mn_2O_3$ | $TiO_2$, $CeO_2$ |
| Condition | $H_2$ | $O_2$ | $CO_2$-$H_2$, $H_2$/$H_2O$ /$CH_3OH$/$N_2$ | $Ti^{3+}$ treatment | $N_2$, $CO_2$, $CH_4$/He | Laser treatment |
| temperature | High-temperature | High-temperature | > 200 °C | Room-temperature | High-temperature | Room-temperature |
| Electronic transfer | Support to metal | Metal to support | Support to metal | Support to metal | Support to metal | Support to metal |
| Suppression of small molecule adsorption | Yes | Yes | Yes | Yes | Yes | Yes |

classical SMSI, such as a wide scope of supports, various construction atmospheres, low heating temperatures, and excellent stability under harsh reaction conditions.

## APPLICATION OF STRONG METAL-SUPPORT INTERACTIONS IN ORR

In general, the requirement for an ideal ORR catalyst includes both high activity and stability. A series of classical SMSI systems, including SMSI, O-SMSI, and A-SMSI catalysis, precisely satisfy the high stability requirement for ORR due to their inherent encapsulation effect. In addition, the electron and mass transfer between metal and support makes the modulation of the catalyst activity more feasible and efficient. For some new types of SMSI, i.e., L-SMSI, wcSMSI, and R-SMSI, their low or room temperature construction strategy and independent encapsulation phenomena can effectively disperse the metal and prevent its detachment and agglomeration, greatly improving the stability of the catalyst.

### Oxide-based materials

TMOs are an ideal alternative to carbonaceous materials as supports for Pt NPs not only because of their robust corrosion resistance but also the strong interaction with the Pt NPs inducing the SMSI effect for enhanced ORR activity and stability enhancement[67]. The SMSI effect mainly arises from an interfacial interaction of Pt-Metal Oxide (Pt-MO), which leads to a modification of the Pt electronic structure and provides several advantages for ORR, including (1) facilitating the $O_2$ adsorption and O-O bond cleavage on the Pt surface; (2) decreasing the OH coverage on the Pt surface; and (3) preventing the detachment and further aggregation of Pt NPs. Based on this, a variety of TMOs have been applied to support Pt-based catalysts toward ORR, such as titanium oxide, cerium oxide, and tungsten oxide.

*Titanium oxide ($TiO_2$)*
Among the various metal oxide supports reported so far, titanium oxide-based materials have been considered as a promising support for nanosized catalysts in the ORR owing to their low cost, nontoxicity, high defect contents, *etc*.[68-70]. The robust corrosion resistance ensures $TiO_2$ is an intrinsically stable electrode material under harsh operation conditions, especially in acid medium and high-temperature environments. Most importantly, the synergetic effect of SMSI between Pt NPs and $TiO_2$ can exquisitely enhance the electrocatalytic performance of Pt NPs and the durability of the catalysts. However, as a support, $TiO_2$ has several drawbacks, such as low electrical conductivity ($10^{-8}$ Scm$^{-1}$) and poor reactivity, limiting the electron interactions between Pt and Ti atoms[71]. Therefore, the issue of insufficient conductivity of $TiO_2$ should be primarily resolved before the application of $TiO_2$ to improve the performance and stability of Pt-based catalysts for ORR.

Coupling $TiO_2$ NPs with superior conductive carbon-based support materials has been reported as one of the most effective solutions to enhance their low electrical conductivity. Wang *et al.* presented a photochemical deposition method for loading Pt NPs onto a composite $TiO_2$-C support (Pt/$TiO_2$-C) and then heated it at 300 °C under $H_2/N_2$ atmosphere for 2 h to induce the SMSI effect[72]. Such a structure enhances not only the overall conductivity of the catalyst system but also the $TiO_2$-induced SMSI effect that strongly encapsulates the Pt NPs to facilitate the electron transfer and prevent the migration and aggregation. As a result, the resulting catalysts exhibit excellent ORR activity and durability in high-temperature environment. Additionally, embedding $TiO_2$ films onto carbon matrix is another fabrication strategy. Shi *et al.* reported a sonochemical reaction method to synthesize a continuous ultrathin (~1.5 nm) $TiO_2$-coated carbon nanotube (CNT) as the support of Pt NPs[73]. Their investigations revealed that the improved ORR activity of Pt/$TiO_2$/C catalysts is attributed to the SMSI effect between Pt NPs and $TiO_2$-coating and the bifunctional mechanism of $TiO_2$. Notably, either $TiO_2$ NPs or a layer in these composites serves as a channel that allows electron transfer between Pt NPs and carbon-based support. Therefore, the $TiO_2$ NPs or coating should not be too big or thick (< 5 nm) to facilitate electrical conductivity. In addition, the $TiO_2$ NPs or coating should also be conformally continuous over the entire carbon surface to prohibit direct contact between the carbon support and the Pt NPs. Therefore, effective tuning of $TiO_2$ particle size or film layers thickness in these composites and selective deposition of Pt NPs in composites are key to improving the SMSI effect and thus increasing the ORR activity and durability of the catalyst.

Recently, an attractive method to enhance the electrical conductivity of titanium dioxide is the introduction of structural defects such as oxygen vacancies ($V_o$) on the surface of $TiO_2$[74], which can construct the Pt-$V_o$-Ti interaction and induce the SMSI effect to optimize the ORR catalytic activity by reducing the desorption free energy of Pt-OH, Pt-O, or $O_2$. In addition, the SMSI effect reduces the binding energy between the active sites and the adsorbed oxygen species, which is beneficial for the ORR process[75]. One common method to introduce $V_o$ in $TiO_2$ is by doping the metal oxides with other metals, such as W[76-78], Nb[78-84], Cr[85,86], Mo[87,88], Ta[89,90], V[91], and more. In general, similar electron donations from the substrate to metals and induced SMSI effect between them can be observed in various doping systems. Synoptically, a screening strategy was proposed by Tsai *et al.* to quickly find out potential supports and dopants ($Ti_{1-x}M_xO_y$ supports, where M = Nb, W, Mo, Ru, *etc.*) in which based on a method of high-throughput DFT calculations[92]. To predict properties by M dopants, a systematic guide map has been produced for $TiMO_2$ substrate that contains data of metal-induced electronic states (MIES, as shown in Figure 6A), the formation energy of oxygen vacancies ($E_{Ovac}$), the adsorption energy of single Pt atoms ($E_{1Pt}$), and charge states of deposited Pt ($\Delta\delta_{Pt}$).

Another effective strategy to enhance ORR performance is to construct nanostructured $TiO_2$ support, such as microspheres, nanofibers, nanotubes, nanosheet assembly, and nanorods. For example, Murphin Kumar *et al.* presented a Pt NPs decorated one-dimensional (1D) $TiO_2$ nanorod (Pt/$TiO_2$ NRs) with remarkably enhanced electronic conductivity and excellent strong coupling of Pt NPs with the $TiO_2$ NRs support compared to the Pt/$TiO_2$(Comm) catalyst (as shown in Figure 6B)[93]. The results verified that the as-prepared Pt/$TiO_2$ NRs composite nanostructures exhibited excellent ORR performance and stability, which are mainly attributed to the unique 1D morphology of the $TiO_2$ NRs providing a greater surface area and the SMSI effect enhancing electron transfer rate at their functional interface.

*Cerium oxides ($CeO_2$)*
Recently, $CeO_2$ has attracted plenty of attention as ORR catalytic support because of its lower price and corrosion resistance in acidic media. What is more, $CeO_2$ support could switch between $Ce^{3+}$ and $Ce^{4+}$ oxidation states due to its abundant oxygen vacancies, which is beneficial to the storage and release of lattice
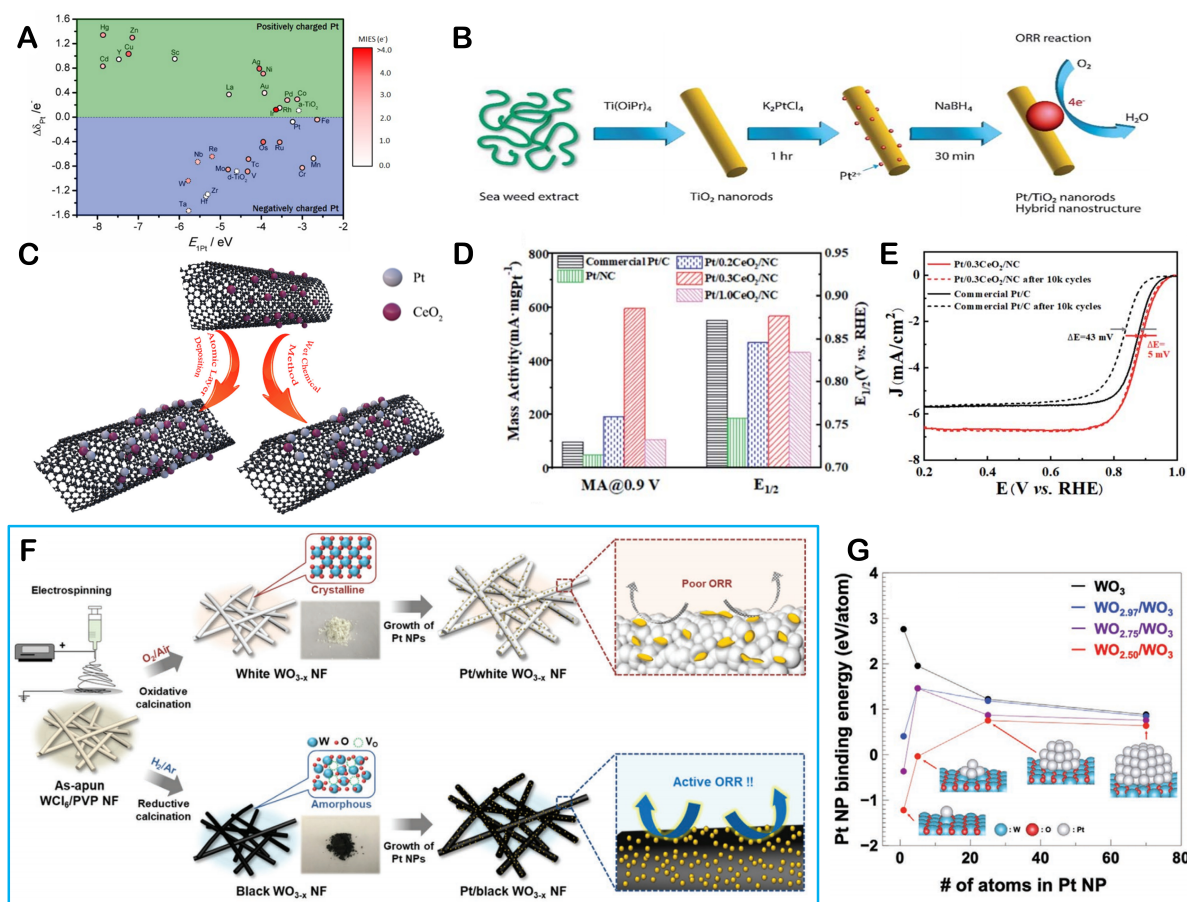
**Figure 6.** (A) A guide map containing four descriptors, MIES, $E_{Ovas}$, $E_{1Pt}$, and $\Delta\delta_{Pt}$ of $TiMO_2$ as the support for Pt catalysts in fuel cells. Reproduced with the permission of Ref.[92] Copyright 2017, Royal Social of Chemistry. (B) Schematic illustrations of the synthesis of Pt/TiO$_2$ NRs catalyst. Reproduced with the permission of Ref.[93] Copyright 2018, Royal Social of Chemistry. (C) Schematic illustrations of the synthesis of Pt/CeO$_2$/CNT junction interface catalyst. Reproduced with the permission of Ref.[95] Copyright 2020, Elsevier. (D) The mass activity (at 0.9V *vs.* RHE) and half-wave potential of commercial Pt/C, Pt/NC, and Pt/xCeO$_2$/NC, (E) LSV curves of Pt/0.3CeO$_2$/NC and commercial Pt/C before and after 10,000 cycles. Reproduced with the permission of Ref.[99] Copyright 2022, Royal Social of Chemistry. (F) Schematic illustrations of the synthesis of Pt/white WO$_{3-x}$ NF and Pt/black WO$_{3-x}$ NF catalysts, (G) Binding energies of Pt NPs of different sizes supported on WO$_{3-x}$ NFs. Reproduced with the permission of Ref.[100] Copyright 2021, John Wiley and Sons.

oxygen, delivering active oxygen species via a spillover process[94]. When the active oxygen species migrate to the surface of Pt NPs, the Pt-CeO$_2$ interfaces will form and accelerate the ORR kinetics. Meanwhile, the oxidation state of Ce$^{3+}$ can also stabilize the Pt NPs and enhance the durability of Pt/CeO$_2$ catalysts. Most importantly, the SMSI effect between Pt NPs and CeO$_2$ support can facilitate the dispersion of Pt NPs and prevent its detachment and aggregation during long-term potential cycling. However, the inferior electronic conductivity of CeO$_2$ has been an obstacle to the widespread use of Pt/CeO$_2$ catalysts in ORR. Similar to TiO$_2$, the introduction of carbon into Pt/CeO$_2$ materials to construct Pt/CeO$_2$/C triple junction interface catalysts has been reported to raise the electronic conductivity without affecting the SMSI between Pt-CeO$_2$ interface (as shown in Figure 6C)[95-97]. With the unique ternary nanostructure, abundant oxygen vacancies, and SMSI effect advantages, the Pt/CeO$_2$/C catalysts exhibit higher ORR performance and durability than commercial Pt/C[98]. Lu *et al.* reported that CeO$_2$/N-C synthesized through a polyol method with an extremely low Pt content (5%) catalyst (Pt/CeO$_2$/N-C) possessed a higher mass activity of 593.6 mA mg$_{pt}$$^{-1}$ when compared with the commercial Pt/C (97.0 mA mg$_{pt}$$^{-1}$) (as shown in Figure 6D)[99]. Meanwhile, the $E_{1/2}$

of $Pt/CeO_2/N-C$ only negatively shifted by 5 mV after a durability test for 10,000 cycles, while it is 43 mV for Pt/C (as shown in Figure 6E). The enhanced ORR activity and durability of $Pt/CeO_2/N-C$ can be attributed to the abundance of oxygen vacancies present on the $CeO_2$ surface, leading to a strong interaction between the $Pt-CeO_2$ interface.

*Tungsten oxides ($WO_3$)*

Tungsten oxide is another metal oxide with superior inherent properties and durability in acidic media. Tungsten trioxide ($WO_3$), as the most stable oxidation state, has been proposed as a promising support for Pt-based electrocatalysts in the ORR due to its series of advantages, which include: (1) the W possesses strong electronegativity, which can modify the electronic structure of Pt and tune the Pt-Pt distance, thereby facilitating the ORR kinetic; (2) $WO_3$ can introduce hydrogen spillover effect on Pt via the formation of hydrogen tungsten bronze ($H_xWO_3$), which speeds up the protonation of the $O_2$ molecule and the rate of oxygen reduction on Pt NPs; (3) the unusual structural defects and unique surface features of $WO_3$ can promote the high dispersion of the Pt NPs and narrow size distribution; (4) the synergistic effect and SMSI effect between Pt and $WO_3$ enable $Pt/WO_3$ catalyst to achieve higher ORR activity and stability. Kim *et al.* synthesized a Pt/black $WO_{3-x}$ nanofiber (NF) catalyst with controlled oxygen deficiency and high electrical conductivity (as shown in Figure 6F)[100]. Their investigations revealed that the as-prepared Pt/black $WO_{3-x}$ NFs exhibited better ORR activity and durability in acidic media as compared to Pt/white $WO_{3-x}$ NFs and Pt/C catalysts. Combined with DFT calculations suggested that the high ORR performance was attributed to plentiful ORR active sites facilitated by numerous oxygen vacancies on the black $WO_{3-x}$ surface and the excellent surface charge properties of the Pt NPs, and the enhanced stability is attributed to the SMSI effect between Pt and oxygen-deficient $WO_{3-x}$ (as shown in Figure 6G). In addition, $Pt/WO_3$-C system catalysts have been reported to have high ORR activity and stability because of the combination of the excellent electrical conductivity of carbon nanomaterials and the strong interaction at the Pt-W interface[101,102]. Interestingly, besides as a support for Pt NPs or a modified part of the carbon substrate, the $WO_3$ has also been applied to modify the catalyst surface. For example, Mo *et al.* prepared a $WO_x$-surface modified PtNi alloy nanowires ($WO_x$-PtNi NWs) catalyst with a high aspect ratio by a one-step solvothermal method, which showed a superior mass activity of 0.85 A $mg_{pt}^{-1}$ at 0.9V than PtNi NWs (0.33 A $mg_{pt}^{-1}$) and Pt/C (0.14 A $mg_{pt}^{-1}$)[103]. Meanwhile, the mass activity of $WO_x$-PtNi NWs only dropped 23.89% after the 30 k cycles durability test, whereas it is 45.94% and 57.9% for PtNi NWs and Pt/C, respectively[104].

Besides $TiO_2$, $CeO_2$, and $WO_3$, other reducible oxide supports, such as $NbO_2$[67] and $Ta_2O_5$[105,106], have also been demonstrated to be capable of enhancing the ORR performance through the SMSI effect with Pt NPs. Some newly published literature for Pt/TMO catalysts with the performance of ORR is given in Table 2. However, in a three-electrode system, a high-speed rotating disc electrode can eliminate the influence of mass transfer and conductivity on the performance of oxide-supported Pt-based catalysts due to the limited conductivity and low specific surface area of oxide supports, however, in practical applications, thicker catalyst layers will require higher mass transfer and conduction capabilities of the catalyst. As a result, there are few reports of Pt-based catalysts supported by oxide carriers for hydrogen fuel cells or metal-air batteries.

**Nitrides-based materials**

TMNs, especially titanium nitride (TiN), niobium nitride (NbN), *etc.*, are used as electrocatalysts because of their excellent electronic conductivity, electrochemical and thermal stability, and corrosion resistance compared with TMOs. In addition, TMNs inherit the characteristics of TMOs in terms of wide source and low price since their synthesis is mainly using TMOs as precursors and roasted under ammonia atmosphere. The excellent corrosion resistance and SMSI facilitate the high catalytic stability and a prolonged lifetime of TMNs-supported catalysts. More importantly, the high electronic conductivity of

**Table 2. ORR performance and stability of Oxide-based supported Pt catalysts**

| Catalyst | Pt (wt.%) | Size of Pt (nm) | Support electrical conductivity (S cm$^{-1}$) | ECSA (m$^2$g$^{-1}_{pt}$) | Mass activity (A mg$^{-1}_{pt}$) | Specific activity (mA cm$^{-2}_{pt}$) | Stability | Ref. |
|---|---|---|---|---|---|---|---|---|
| **TiO$_2$-based catalysts** | | | | | | | | |
| Pt/TiO$_2$ | 12 | 30 | / | 7.23 | 0.083 | 1.134 | 5.9% loss of ECSA after 5,000 cycles | [68] |
| Pd/TiO$_2$/C | / | 7.8 | / | 54.2 | 2.6 | 4.8 | 13% mass activity loss after 10,000 cycles | [69] |
| PtAu/TiO$_2$ NWs | / | 3.62 | / | 85.8 | 0.381 | 0.441 | 20% loss of ECSA after 5,000 cycles | [70] |
| Pt/TiO$_2$-C | 3.5 | 3.5 | / | 82 | 0.205 | / | 0.8% loss of ECSA after 10,000 cycles | [72] |
| Pt/TiO$_2$/C | 4.4 | 2.3 | / | 50.2 | 0.442 | 0.881 | 2.3% loss of ECSA after 10,000 cycles | [73] |
| Pt/TiWN$_x$O$_y$ | 20 | 9 | 2.3 | / | 0.1 | / | 22.9% mass activity loss after 5,000 cycles | [78] |
| Pt/TiNbO$_2$ NTs | 6 | 4 | / | 110.3 | 0.314 | / | 19% loss of ECSA after 2,000 cycles | [84] |
| Pt/TiCrO$_2$ | / | 3-5 | / | 18 | / | 0.46 | / | [86] |
| Pt/TiMoO$_2$ | 20 | 3-4 | 2.8 × 10$^{-4}$ | 72.5 | / | / | 8% loss of ECSA after 5,000 cycles | [87] |
| Pt/TiTaO$_2$ | 20 | | 0.2 | | 0.06 | / | 35% loss of ECSA after 10,000 cycles | [89] |
| Pt/TiVO$_2$ | 6 | 2.0 | / | 115.4 | 0.356 | / | 24% mass activity loss after 4,000 cycles | [91] |
| Pt/TiO$_{2-x}$ NSs | / | 3 | 2.66 × 10$^{-3}$ | 65 | 0.006 | 13.27 | 32% loss of ECSA after 10,000 cycles | [93] |
| **CeO$_2$-based catalysts** | | | | | | | | |
| Pt/CeO$_2$/CNT | 10 | 2.5/3.7 | | 74.1 | ~0.38 | / | 13.4% mass activity loss after 5,000 cycles | [95] |
| Pt/CeO$_2$/C | / | 2-3 | / | 50.1 | 0.05 | / | 80% loss of ECSA after 10,000 cycles | [97] |
| Pt/CeO$_2$N-C | 5.6 | 5.7 | / | / | 0.238 | 5.88 | / | [98] |
| Pt/CeO$_2$-NC | 5 | 2.3 | / | / | 0.6 | 6.72 | 5 mV E$_{1/2}$ loss after 10,000 cycles | [99] |
| **WO$_3$-based catalysts** | | | | | | | | |
| Pt/black WO$_{3-x}$ | / | 5 | / | / | / | / | 13% loss of ECSA after 5,000 cycles | [100] |
| Pt/WO$_3$ | 20 | 2-3 | 7.8 ×10$^{-3}$ | 75 | 0.325 | 0.769 | 5.5% loss of ECSA after 5,000 cycles | [101] |
| WO$_{x-(0.25)}$-PtNi NWs/C | / | 2-3 | / | 77.5 | 0.45 | 0.58 | 15.72% loss of ECSA after 30,000 cycles | [103] |
| **Other oxygen-based catalysts** | | | | | | | | |
| Pt/NbO$_2$/C | / | 5.3 | / | 66 | 0.56 | 0.85 | 15% loss of ECSA after 5,000 cycles | [67] |
| Pt/N-ALDTa$_2$O$_5$/C | / | 3.3 | 85.7 | 70.3 | 0.28 | / | 14.9% mass activity loss after 10,000 cycles | [105] |
| Pt-Ta$_2$O$_5$/CNT | 9.06 | 3 | 5.8 × 10$^{-5}$ | 78.4 | 0.23 | 0.293 | 3.5% loss of ECSA after 10,000 cycles | [106] |

TMNs eliminates the disadvantage of the inherent poor conductivity in TMOs-supported catalysts. Furthermore, recent studies have demonstrated the TMN itself possesses considerable ORR catalytic activity under acidic conditions. Therefore, TMNs-supported Pt-based catalysts display not only excellent ORR

activity and stability but also hold significant potential for use in fuel cell and metal-air battery devices.

### Titanium nitride (TiN)

TiN as a high conducting material (119 $Scm^{-1}$ as opposed to 5 $Scm^{-1}$ for carbon black) has been recently reported as a promising alternative candidate to the carbon-based support for Pt NPs due to its good thermal stability, high corrosion- and structure-resistance, and electrochemically stable in fuel cell operating conditions[107]. Also, the SMSI effect between TiN support and Pt NPs has been confirmed to be capable of supplying a strong adhesion to Pt NPs and accelerating electron transfer. Since Ni doping may boost the ability of Ti atoms to transfer electrons to the adsorbed oxygen molecules and simultaneously reduce the Ti-O strength to an appropriate level, thereby resulting in high ORR activity[33,108]. As an example, a marriage of the high activity of the Pt shell and the low cost and superb stability of core TiN NPs was obtained by Tian *et al.* via depositing several atomic layers of thick Pt shell on a binary titanium nickel nitride nanocrystal (as shown in Figure 7A)[109]. The TiNiN@Pt catalyst exhibited extremely high activity and excellent durability for the ORR in the acidic solution owing to the synergetic effects of SMSI between the ultrathin Pt skin and the ultrastable TiNiN support. However, a series of inter-particle grain boundaries may act as electron reservoirs and traps during the electron transfer between TiN support and Pt NPs, resulting in the size of TiN particles decreasing and thereby losing their intrinsic high electrical conductivity. To solve this problem, Shin *et al.* designed a grain-boundary-free scaffold-like porous TiN nanotube (NT) with high electrical conductivity (ca. 30-fold higher than TiN NPs) as a support for Pt NPs (as shown in Figure 7B)[110]. The result showed that the Pt/TiN NT exhibited a higher ORR activity and stability compared with Pt/TiN NPs catalyst because of the unique hollow and porous, scaffold-like, cylindrical structure of TiN NT, which allows for facilitated carrier diffusion in TiN materials, resulting in improved electrical conduction. To date, a series of TiN modifications through nanostructure formation of nanotubes[111-115], nanoflakes[116,117], nanorods[118], nanosphere[119] (as shown in Figure 7C-F, respectively.) and through doping by Nb[120], Mo[121], Cu[122], Co[113,118], Cr[114,123], and Ni[124] were reported to modify the metal-support interface structure, modulate the activation energy of molecular adsorption, and enhance interfacial electron transfer and mass transfer, thereby improving the ORR activity and stability of catalysts.

### Vanadium nitride (VN)

Vanadium nitride (VN), a kind of transition metal nitride, has received much attention in the field of supercapacitors and lithium-ion batteries but less attention in ORR since most of the synthesis methods of VN involve high-temperature calcination, which inevitably leads to agglomeration of particles, resulting in lower specific areas. Therefore, it is necessary to seek a breakthrough from the synthesis of VN materials to achieve the expected level of ORR activity of catalysts for Pt/VN systems. Yin *et al.* successfully synthesized a VN/graphitic carbon (GC) nanocomposite for the first time, which acts as an enhanced support of Pt NPs toward ORR[125]. After loading 10% Pt NPs, the resulting Pt-VN/GC catalyst demonstrates higher ORR activity than 20% Pt/C. More importantly, the electrochemically active surface area (ECSA) of 10% Pt-VN/GC catalyst maintains 99% after 2,000 cycles, whereas Pt/C is just 75%. The excellent stability is attributed to the synergistic and SMSI effects between VN and Pt and the stability of the GC. Recently, a high electrical conductivity VN NFs support Pt NPs catalyst (Pt/VN) was prepared by Kim *et al.* (as shown in Figure 7G)[126]. The Pt/VN catalysts exhibited higher ORR activity and durability in acid electrolytes compared to Pt/C. DFT calculations provided further evidence of the SMSI effect between Pt and VN, which contributed to the excellent stability of the catalyst (as shown in Figure 7H).

### Chromium nitride (CrN)

Chromium nitride (CrN) is also a viable support material and possesses several desirable properties, including high electrical conductivity, outstanding thermal and electrochemical stability, exceptional
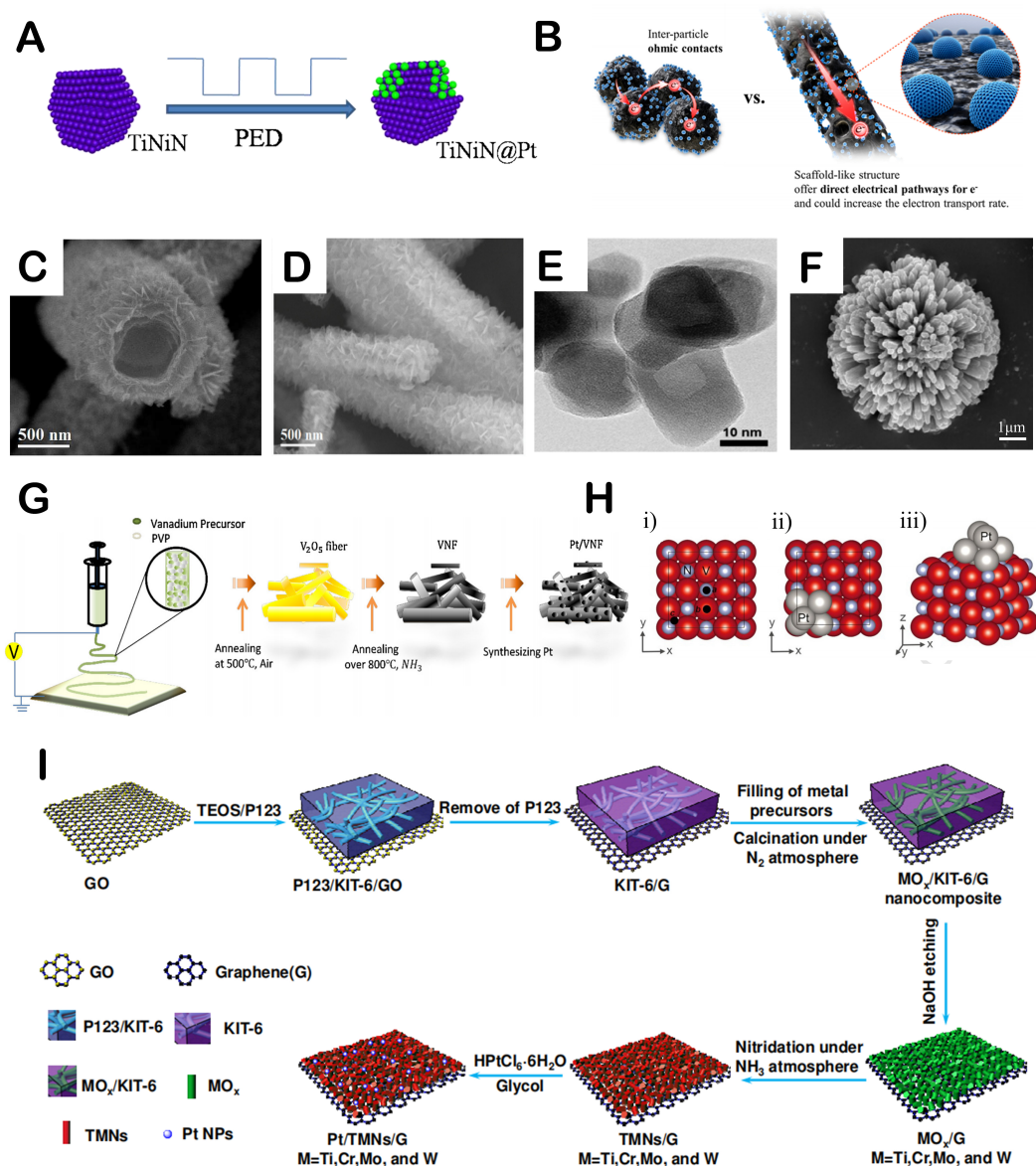
**Figure 7.** (A) Schematic illustrations of the synthesis of TiNiN@Pt catalyst. Reproduced with the permission of Ref.[109] Copyright 2016, American Chemical Society. (B) Schematic illustrations of Pt/spherical TiN NPs and Pt/scaffold-like TiN NTs catalysts, Reproduced with the permission of Ref.[110] Copyright 2016, American Chemical Society. SEM images of (C) $Ti_{0.9}Ni_{0.1}N$ nanotubes. Reproduced with the permission of Ref.[124].Copyright 2018, Royal Social of Chemistry, (D) $Ti_{0.9}Cu_{0.1}N$ nanoflakes. Reproduced with the permission of Ref.[116] Copyright 2018, Elsevier, (E) TiN nanorods. Reproduced with the permission of Ref.[110].Copyright 2016, American Chemical Society, (F) TiN nanosphere. Reproduced with the permission of Ref.[119] Copyright 2022, Elsevier. (G) Schematic illustrations of the synthesis of Pt/VN catalyst. (H) (i) Adsorption sites of $Pt_1$ or $Pt_6$ on the VN surface (ii and iii) top view and side view of the $Pt_6$-VN system, respectively. Reproduced with the permission of Ref.[126] Copyright 2017, Elsevier. (I) Schematic illustrations of the synthesis of 2D layered mesoporous Pt/TMNs/G catalysts. Reproduced with the permission of Ref.[130].Copyright 2016, American Chemical Society.

hardness and corrosion resistance, and good catalyst-support interaction[127]. Yang *et al.* reported mesoporous CrN-supported Pt NPs (Pt/CrN) catalysts and found that, as compared with the commercial Pt/C catalysts, the obtained Pt/CrN catalysts exhibited both higher ORR activity and stability due to the smaller pore size and higher surface area of the CrN support and the SMSI effect between Pt and CrN[128,129]. Subsequently, Liu *et al.* constructed a series of 2D layered mesoporous TMNs/graphene including mono-

TiN/G, CrN/G, WN/G, MoN/G, and binary-TiCrN/G, TiWN/G and TiMoN/G nanocomposites with a large surface, high porosity, and excellent electrical conductivity (as shown in Figure 7I)[130]. After loading Pt NPs, the binary Pt/Ti$_{0.5}$Cr$_{0.5}$N/G catalysts exhibit the best ORR activity and stability due to the enhanced exposure of active sites, the large accessible active sites, and the improved specific surface area and porosity, resulting in strengthened electron transfer between Pt, Ti$_{0.5}$Cr$_{0.5}$N, and graphene.

From the above results, it is clear that the use of TMNs as support is an effective method to enhance the ORR activity and stability of Pt-based catalysts. Firstly, the overall structural stability of the catalyst can be enhanced by the SMSI between TMN and Pt. In addition, the inherent ORR performance and excellent electrical conductivity of TMNs can further promote the catalytic activity in TMNs-supported Pt catalyst systems. Moreover, the ORR catalytic activity can be further enhanced by doping TMN supports with other elements due to the modulated structure and composition of the supported Pt nanomaterials. The detailed ORR performance of Pt/TMN catalysts is presented in Table 3.

**Carbides-based materials**
Apart from TMO and TMN, TMC also possesses the potential as the ORR catalyst support because of their chemical stability and high electrical conductivity. First, the similar electronic structure and catalytic properties of TMC and Pt-group metals can reduce the overall loading of precious metals. Second, Pt-based metals tend to bind firmly to metal-terminated TMC surfaces and facilitate the electron transfer with its support to improve ORR stability and intrinsic activity[131-133].

*Titanium carbide (TiC)*
Titanium carbide (TiC) possesses similar structural and physicochemical properties as TiN. This results in a strong interaction between the TiC support and the Pt nanoclusters, which leads to an increase in the adsorption strength of the oxygen molecules on the Pt surface and improves the ORR activity of the Pt/TiC catalyst. According to the DFT calculations, the TiC support can strongly anchor Pt NPs and prevent their exfoliation or agglomeration due to the formation of Pt-C-Ti bonds (as shown in Figure 8A)[134]. Moreover, Pt-C-Ti bonds were also demonstrated to possess stronger electronic interaction as compared to Pt-N-Ti and Pt-O-Ti bonds, which leads to higher accessibility of active Pt sites in Pt/TiC and presents a better ORR activity and stability than Pt/TiN and Pt/TiO$_2$ catalysts[71]. Lee *et al.* synthesized a high conductive two-dimensional Ti$_3$C$_2$ (MXene)-supported Pt NPs catalyst (Pt/Ti$_3$C$_2$) and precisely tuned the number of layered Ti$_3$C$_2$ to provide more electron transfer for Pt NPs[135]. DFT calculation showed that electron-rich Pt had fewer *d*-band vacancies, weakening the binding of oxygen species to the Pt surface and increasing the rate of *OH desorption. Furthermore, the electron transfer between Pt and Ti$_3$C$_2$ triggers the SMSI effect, inducing encapsulation phenomena of metal support and ensuring the stability of the Pt/Ti$_3$C$_2$ catalysts. Subsequently, Xie *et al.* presented a Pt/ Ti$_3$C$_2$X$_2$ (X = OH, F) catalyst and found that the -OH and -F groups can also prevent Pt NPs from agglomeration, Ostwald ripening, and dissolution, as does SMSI effect[136]. Nevertheless, the TiC substrate is not electrochemically stable and will undergo irreversible electrochemical oxidation. To solve this problem, a Pt$_3$Pd/TiC@TiO$_2$ core-shell composite catalyst has been reported to possess better ORR stability than that of Pt/TiC and Pt$_3$Pd/TiC catalysts by Ignaszak *et al.* due to the TiO$_2$ shell can act as a protective layer over the TiC core[137]. Besides the core-shell protection strategies, electrochemical modification is another effective method to obtain oxygen-rich species on catalyst surfaces. A surface aluminum-leached Ti$_3$AlC$_2$-supported Pt NPs catalyst (Pt/e-TAC) with much-improved ORR activity and stability compared to Pt/C has been synthesized by Xie *et al.* (as shown in Figure 8B)[138]. DFT calculations indicated that the enhancement mechanism of Pt/e-TAC is attributed to the stronger interaction that exists between Pt$_{13}$ clusters and Ti$_3$C$_2$ with respect to C. The partial density of states (PDOS) confirmed that the SMSI effect between Pt and Ti$_3$C$_2$ results in a considerable overlap between the Pt-d and Ti-d states near the Fermi energy level.

**Table 3. ORR performance and stability of Nitrides-based Pt catalysts**

| Catalyst | Pt (wt.%) | Size of Pt (nm) | Support electrical conductivity (S cm$^{-1}$) | ECSA (m$^2$g$^{-1}_{pt}$) | Mass activity (A mg$^{-1}_{pt}$) | Specific activity (mA cm$^{-2}_{pt}$) | Stability | Ref |
|---|---|---|---|---|---|---|---|---|
| **TiN-based catalysts** | | | | | | | | |
| TiNiN@Pt | 4.98 | 2-3 | / | 97 | 0.83 | 0.49 | 21% loss of ECSA after 10,000 cycles | [109] |
| Pt/TiN NTs | 20 | 3.65 | 118 | 61.3 | 0.21 | 3.37 | No degradation ECSA after 10,000 cycles | [110] |
| Pt/TiN NTs | 20 | 3.75 | 85 | 45.8 | 0.4 | 0.87 | 23% loss of ECSA after 12,000 cycles | [111] |
| Pt/Ti$_{0.95}$Co$_{0.05}$N | 20 | 3.34 | / | 51.5 | 0.84 | / | 14% loss of ECSA after 10,000 cycles | [113] |
| Pt$_3$Cu/TiN NTs | 20 | 28 | 184 | 45.7 | 2.43 | 5.32 | 16.1% mass activity loss after 10,000 cycles | [115] |
| Pt/Ti$_{0.9}$Cu$_{0.1}$N NFs | 20 | 2.3 | / | 57.5 | 1.56 | 2.64 | 13% loss of ECSA after 10,000 cycles | [116] |
| Pt/TiN NPs | 20 | 3.0 | 679 | / | 0.65 | 1.06 | 12% loss of ECSA after 15,000 cycles | [117] |
| TiN@Pt | 12 | 2-3 | / | 66 | 0.44 | 0.33 | 10% loss of ECSA after 3,000 cycles | [119] |
| Pt/Ti$_{0.8}$Mo$_{0.2}$N | 20 | 3.4 | / | 54.9 | 0.62 | 1.07 | 47% loss of ECSA after 9,000 cycles | [121] |
| Fe$_3$Pt/Ti$_{0.5}$Cr$_{0.5}$N | 10.5 | 1-2 | / | 52.8 | 0.68 | 1.28 | 21.8% mass activity loss after 5,000 cycles | [123] |
| Pt/Ti$_{0.9}$Ni$_{0.1}$N NTs | 20 | 3.1 | / | 59.7 | 0.78 | 1.3 | 9% mass activity loss after 15,000 cycles | [124] |
| **VN-based catalysts** | | | | | | | | |
| Pt-VN/GC | 10 | 3.8 | / | 12.6 | 0.137 | / | 1% loss of ECSA after 2,000 cycles | [125] |
| Pt/VN | 15 | 2-8 | / | / | / | / | / | [126] |
| **CrN-based catalysts** | | | | | | | | |
| Pt/Ti$_{0.95}$Cr$_{0.05}$N NTs | 20 | 3.0 | / | 52 | 0.62 | / | 29% loss of ECSA after 1,800 cycles | [114] |
| Pt/CrN | 20 | 3.9 | 69 | 75.3 | 0.009 | 0.012 | 30% mass activity loss after 10,000 cycles | [128] |
| Pt/Ti$_{0.5}$Cr$_{0.5}$N$_2$/G | 15.6 | 4 | / | 76.2 | 0.79 | 1.04 | 9.3% loss in the acidic medium after 1,800 cycles | [130] |

*Molybdenum carbide (Mo$_2$C)*

Molybdenum carbide (Mo$_2$C) is another carbide material that has received a lot of interest as a support for Pt-based catalysts[139-142]. Elbaz *et al.* synthesized a Pt/Mo$_2$C catalyst with unique platinum rafts consisting of 6 atoms or less on the Mo$_2$C surface, which showed a higher mass activity of 0.29 A mg$^{-1}_{pt}$ at 0.9 V than Pt/XC-72 (0.19 A mg$^{-1}_{pt}$). Meanwhile, the Pt/Mo$_2$C lost only 10% of its initial ECSA, whereas the Pt/XC-72 lost approximately 80% after 5,000 cycles of accelerated durability testing[143]. Subsequently, they investigated the formation of Pt nanorafts and its ORR catalytic activity on Mo$_2$C using first-principles calculations and found that the O-O repulsion between the O atoms on the Mo$_2$C and the O adsorbate enhances the ORR activity by weakening the O adsorption energy. Moreover, the SMSI effect and strong binding energy between Pt and Mo$_2$C are prone to show better electrocatalytic activity towards ORR when compared to Pt/XC-72 (as shown in Figure 8C)[144]. More recently, Mo$_2$C has been demonstrated as a promising support material for anchored Pt single atoms, as the Mo atoms can provide SMSI with Pt species. Significantly, it is able to anchor Pt single atoms over a broad range of concentrations, thereby
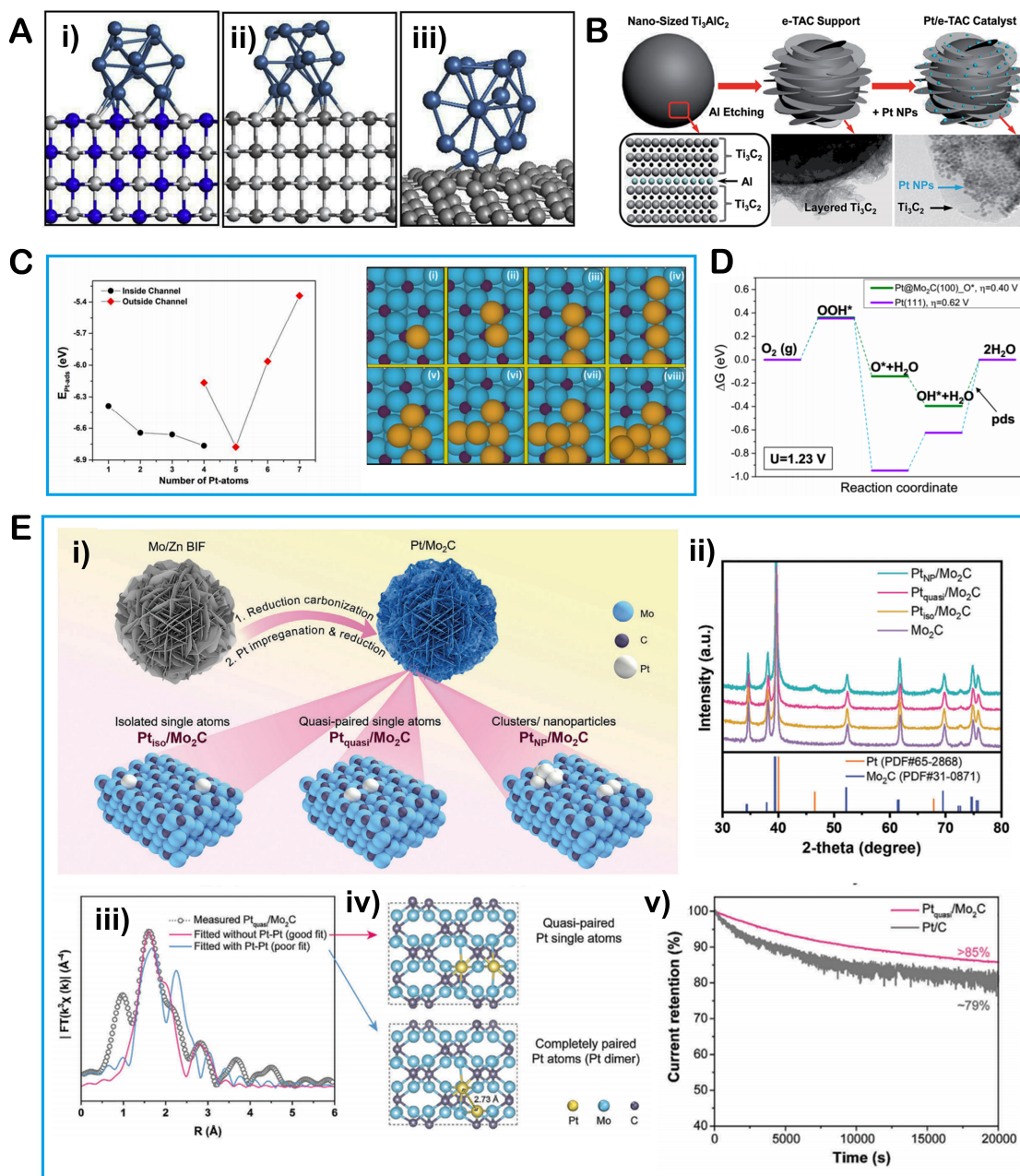
**Figure 8.** (A) Stable structure models of $Pt_{13}$ clusters on (i) TiN, (ii) TiC, and (iii) graphene. Reproduced with the permission of Ref.[134] Copyright 2019, Elsevier. (B) Schematic of Pt/e-TAC catalyst formation. Reproduced with the permission of Ref.[138].Copyright 2014, Royal Society of Chemistry. (C) Binding energies of Pt atoms on the ordered $Mo_2C$ surface and the formation of Pt nanorafts on the $Mo_2C$ surface (i) to (iv) Pt deposited growing in a channel, (v) to (viii) Pt atoms deposited outside the channel with an increase in Pt-loading. Purple, blue, and yellow spheres represent C, Mo, and Pt atoms, respectively. Reproduced with the permission of Ref.[144] Copyright 2018, American Chemical Society. (D) Free energy diagrams of ORR on $Pt@Mo_2C(100)\_O^*$ and Pt(111). Reproduced with the permission of Ref.[148].Copyright 2021, American Chemical Society. (E) Schematic diagram, phase characterization, and performance. (i) Schematic illustrations of the synthesis of various $Pt/Mo_2C$ samples, (ii) XRD patterns of various $Pt/Mo_2C$ samples, (iii) Fitted EXAFS results of $Pt_{quasi}/Mo_2C$, without and with Pt-Pt coordination, (iv) Structural models of the cases for quasi-paired Pt single atoms and completely paired Pt atoms, (v) Stability of $Pt_{quasi}/Mo_2C$ determined by chronoamperometry test conducted at a potential of 0.85 V. Reproduced with the permission of Ref.[149] Copyright 2021, John Wiley and Sons.

allowing the modeling of potential synergistic interactions among the densely populated Pt single atoms without affecting the dispersion and durability[145-147]. Huang *et al.* successfully dispersed a series of TM

atoms, including Pt, Pd, Ir, *etc.* atoms, over $Mo_2C$ by bonding with its surface Mo atoms to obtain thermodynamically stable single-atom catalysts (SACs) and investigated their corresponding ORR activity and selectivity based on DFT calculations[148]. It is found that only Pt@$Mo_2C$ exhibits extraordinary 4e⁻ ORR activity with an overpotential of only 0.33 V, exceeding the state-of-the-art Pt (111) catalyst (as shown in Figure 8D). Zhang *et al.* reported a $\beta$-$Mo_2C$ support quasi-paired Pt single atoms catalyst ($Pt_{quasi}$/$Mo_2C$), that is, two closely neighboring and yet non-contiguous Pt sites exhibit synergistic interactions while remaining "single" (as shown in Figure 8E (i))[149]. Similar to the isolated Pt single atoms, there is no crystalline Pt phase in the X-ray diffraction (XRD) pattern, and no Pt-Pt bond is present (as shown in Figure 8E (ii-iv)). The $Pt_{quasi}$/$Mo_2C$ catalyst showed higher stability as compared to Pt/C, with a current density retention of more than 85% after 20,000s (as shown in Figure 8E (v)), which was attributed to the synergistic interaction from the two quasi-paired Pt atom sites in modulating the binding mode of reaction intermediates as well as the SMSI between Pt and $Mo_2C$. Nowadays, $Mo_2C$-supported Pt single-atom catalysts are at the forefront of research and promising for practical applications in PEMFCs.

Besides TiC and $Mo_2C$, a series of carbides (TaC[150], WC[151,152], NbC[153,154], ZrC[13,155], *etc.*)-supported Pt-based catalysts have also been reported to exhibit excellent ORR performance due to SMSI effect. Some recently published literature on the ORR performance of Pt/TMCs is summarized in Table 4. In addition, similar to TMNs, it is possible that these carbides may act as catalytic centers themselves. This outcome would be desirable because the parent metals of most TMC are orders of magnitude more abundant in the earth's crust and less expensive than Pt-based metals[156]. However, the carbide particle structure itself and the surface area make the system even more complex. In addition, the nucleation and growth mechanism of catalyst particles on the carbide surfaces is not fully understood at present, and the effects of surface functional groups, surface defects, and relative catalyst particle distribution still need further investigation. Moreover, carbon corrosion has been a drawback for the commercial application of Pt-based catalysts supported by TMCs. Future work should pay more attention to the durability of the TMCs-supported catalysts, especially in a realistic PEMFC cathode environment under working conditions, and elucidate the corrosion mechanisms and durability behavior.

## Other non-carbon supporting materials

### *Transition metal sulfide*

Presently, 2D layered transition metal chalcogenides (TMS), especially $MoS_2$, have been used as potential supports for Pt-based catalysts because of their unique layer structures, abundant defects, and edge locations[157,158]. Bothra *et al.* have systematically explored the ORR activity of different size $(Pt)_n$ clusters ($n$ = 1-12) supported $MoS_2$ by first-principles density functional theory. This scaling relationship gives rise to a model volcano curve (as shown in Figure 9A), indicating that $Pt_7$/$MoS_2$ is the best electrocatalyst for ORR with a minimum overpotential value of 0.33 V, which is highly dependent on the binding strength of the oxygenated species and can be correlated with electron transfer between Pt and $MoS_2$[159]. Therefore, the restacking behavior of the $MoS_2$ layer reduces the anchoring sites for Pt deposition and does not provide high catalytic activity for PEMFC applications. To solve this issue, Anwar *et al.* introduced $MoS_2$ into a graphene with a mesh shape and electronic conductivity to prepare a hybrid support material ($MoS_2$-rGO) for a Pt-based catalyst. The results show that the abundantly exposed edges of the $MoS_2$ NPs constitute a homogeneous dispersion of Pt NPs, the mesh structure of graphene prevents the leaching of the Pt NPs, and the outstanding electronic conductivity of the r-GO cooperatively leads to the higher electrochemical performance[160]. Subsequently, a flowerlike $MoS_2$/N-doped reduced graphene oxide supported ultrafine Pt NPs catalyst (Pt@$MoS_2$/NrGO) was successfully synthesized by Logeshwaran *et al.*[158]. The purpose of incorporating N atoms into r-GO is to enhance its conductivity and catalytic activity owing to the high-electron transport kinetics and the capability to inhibit Pt NPs from agglomerating on the support.

**Table 4. ORR performance and stability of Carbide-based Pt catalysts**

| Catalyst | Pt (wt.%) | Size of Pt (nm) | Support electrical conductivity (S cm$^{-1}$) | ECSA (m$^2$g$^{-1}_{pt}$) | Mass activity (A mg$^{-1}_{pt}$) | Specific activity (mA cm$^{-2}_{pt}$) | Stability | Ref |
|---|---|---|---|---|---|---|---|---|
| **TiC-based catalysts** | | | | | | | | |
| Pt/Ti$_3$C$_2$X$_2$ | 20 | 3-7 | 1.2 × 10$^{-5}$ | 54.88 | / | / | 15.66% loss of ECSA after 10,000 cycles | [136] |
| Pt$_3$Pd-TiC-TiO$_2$ | / | 3.15 | 0.12 | 37.6 | 0.33 | 0.883 | 20% loss of ECSA after 2,000 cycles | [137] |
| Pt/Ti$_3$AlC$_2$ | 14.8 | 2 | 4.3 × 10$^{-2}$ | 44.81 | 0.18 | 0.399 | No degradation ECSA after 1,500 cycles | [138] |
| **M$_2$C-based catalysts** | | | | | | | | |
| Pt-Mo$_2$C/CNTs | 16 | 3-6 | / | / | / | / | / | [139] |
| Pt/Mo$_2$C-F | / | 3.25 | / | 58.5 | 0.149 | 0.024 | 35% loss of ECSA after 5,000 cycles | [142] |
| Pt/M$_2$C | 5 | 1 | / | / | 0.29 | / | 10% loss of ECSA after 5,000 cycles | [143] |
| Pt$_{quasi}$/Mo$_2$C | 2.36 | / | / | / | 0.224 | / | over 85% retention of current density after 20,000 s | [149] |
| **Other carbide-based catalysts** | | | | | | | | |
| ALD-Pt-ZrC | 19 | 2-4 | / | / | 0.12 | 0.23 | 17% loss of ECSA after 4,000 cycles | [13] |
| Pt-Ta$_2$O$_5$.TaC | 4.95 | 2.4 | / | 70 | 0.297 | 0.424 | 5.7% loss of ECSA after 10,000 cycles | [150] |
| Pt-Ni/WC | 9.425 | 4 | / | 178.4 | 2.198 | 1.232 | 9.19% loss of ECSA after 3,000 cycles | [152] |
| Pt/NbC/C | 30 | 3.1 | 10 | 52 | 0.087 | / | 31% loss of ECSA after 10,000 cycles | [153] |

Moreover, the attachment of MoS$_2$ between NrGO and Pt NPs also generates a synergistic effect and SMSI effect, resulting in Pt@MoS$_2$/NrGO catalysts exhibiting superior ORR activity and stability, with a half-wave potential at 0.895 V and only 1.7% loss after 30 k ADT in 0.1 M HClO$_4$ solution, which is greater than that of commercial Pt/C by a factor of 0.876 V and 3% loss, respectively. Currently, Pt-based/TMS catalysts are extensively employed in hydrogen evolution reaction (HER), while the catalyst activity in oxygen evolution reaction (OER) and ORR has been limited, mainly because the TMS supports offer poor reactivity, slow electronic conductivity, and fast reunion rate of electrons and holes[161].

*Transition metal phosphide and boride*
Transition metal phosphide and boride (TMP and TMB) themselves as excellent catalysts have been investigated extensively for HER, OER, and ORR. However, there is still a lack of relevant work and understanding to design the TMP- and TMB-supported Pt-based catalyst[162,163]. Zirconium phosphates (ZrP)-supported Pt NPs catalysts have recently been reported that ORR benefited from the phosphate groups in ZrP has acidic functionality, and thus the close contact with Pt NPs can facilitate the active interface (as shown in Figure 9B). The Pt/ZrP catalyst shows strong evidence of charge transfer from the ZrP support to Pt NPs, contributing to SMSI effect, and in turn directly affecting the adsorption strength of the oxygen and oxygen intermediates[164]. Titanium diboride (TiB$_2$), as an electrically conducting ceramic material, is a promising support medium for PEMFC catalysts thanks to their low resistance and considerable chemical stability. In previous work, Yin *et al.* successfully prepared Pt/TiB$_2$ catalyst via a colloidal route and revealed that the durability of

**Figure 9.** (A) Thermodynamic volcano relation for ORR activity as a function of Gibbs adsorption energy of *OH. Reproduced with the permission of Ref.[159] Copyright 2016, Royal Society of Chemistry. (B) Schematic illustrations of the synthesis of the Pt/ZrP catalysts. Reproduced with the permission of Ref.[164] Copyright 2023 John Wiley and Sons. (C) Schematic diagram of Pt NPs anchored on $Ti_3C_2T_x$ layer Reproduced with the permission of Ref.[168] Copyright 2020, Elsevier. (D) The radar chart of the performance of TMO, TMN, and TMC supports.

Pt/TiB$_2$ was approximately four times better than that of the commercial Pt/C catalyst[165]. However, the large particle size (1~8 μm) and the low BET surface area of the raw TiB$_2$ support severely hinder the deposition of Pt NPs. Subsequently, they employed perfluorosulphonic acid as both a proton-conducting polymer and a stabilizer to strengthen the SMSI between the Pt NPs and the TiB$_2$ support, enabling the Pt NPs to be strongly anchored and effectively dispersed on the inert ceramic support[166]. In the other proposal, Huang *et al.* made defects on the surface of TiB$_2$ support by H$_2$O$_2$ etching to create abundant active sites or functional groups to help the deposition of Pt[167]. The results showed that the mass activity of Pt/H$_2$O$_2$-TiB$_2$ was 80.3 mA mg$^{-1}$, which was significantly higher than that of Pt/TiB$_2$ at 2.9 mA mg$^{-1}$.

Although TMP- and TMB-supported Pt-based catalysts have been demonstrated as promising ORR catalysts, their characteristics of limited conductivity and easy agglomeration cause them to still have a long way for practical application. Therefore, anchoring them to a conducting substrate may be an effective strategy to overcome these shortcomings in the future.

*MXenes*

MXenes are novel two-dimensional (2D) graphene-like transition metal carbides and/or nitrides that have been developed as competitive candidates for electrocatalyst support for PEMFC applications due to their

unique layer structures, excellent electronic properties (approximately 15,100 S/cm), and high corrosion resistance, which facilitate various electrochemical reactions[168-170]. Among the MXene families, $Ti_3C_2T_x$ support is the most commonly used and expected to supply a strong adhesion for Pt NPs, benefiting from their same elemental composition as TiC[171]. Zhang *et al.* reported the presence of abundant -OH and -F surface termination groups on $Ti_3C_2T_x$, which makes it easier to create Pt deposition sites (as shown in Figure 9C). Thanks to the SMSI effect between Pt NPs and $Ti_3C_2T_x$ nanosheets, the migration and agglomeration of Pt NPs is effectively prevented, leading to $Pt/Ti_3C_2T_x$ catalysts that exhibit superior ORR activity and stability over commercial Pt/C in both acidic and alkaline environments[168]. However, the charge-transfer performance of the $Ti_3C_2T_x$ surface with the functional groups may be limited by the inherent restacking phenomenon of 2D materials. Hybridization of $Ti_3C_2T_x$ with carbon nanotube (CNT) is an effective strategy to prevent the agglomeration of the $Ti_3C_2T_x$ support caused by strong van der Waals forces and enhance electron transport between $Pt-Ti_3C_2T_x$-C. Xu *et al.* demonstrated that the hybridized $Pt/CNT-Ti_3C_2T_x$ shows excellent ORR activity (the mass activity is 3.4-fold over Pt/C) and durability (a great ECSA retention of 94% with respect to that in Pt/C of 73% after 2,000 cycles accelerated stress test (AST))[172]. Furthermore, the $Pt/CNT-Ti_3C_2T_x$ exhibited the peak power density (181 mW cm$^{-2}$) in the single-cell MEA test compared to Pt/CNT, $Pt/Ti_3C_2T_x$, and Pt/C, attributed to the better mass transport on this cathode material[172]. In addition to $Ti_3C_2T_x$, Yang *et al.* revealed that $V_2C$ MXene displays excellent charge transfer kinetics and conductance[173]. The SMSI effect enables highly dispersed Pt atoms and thin Pt films to form on the $V_2C$, dramatically improving the stability of $Pt/V_2C$ MXene towards the ORR[173,174]. Li *et al.* have identified $Nb_2CT_x$ as capable of providing a good catalytic support interaction for Pt through an efficient method of generating reactive metal-support interactions on $Pt/Nb_2CT_x$ catalysts at moderate temperature[175]. Although the use of MXene as Pt-based catalyst support has pointed out the direction to ORR, the AST is still unsatisfactory, possibly due to the oxidative environment of the fuel cell cathodes, which exposes MXene to oxidation over an extended period of time. Future designs could consider incorporating nanomaterials such as carbon nanostructures into MXene to improve its oxidative stability.

Finally, while several PGM catalysts have shown impressive ORR activity in half-cell tests, few of them have demonstrated both good activity and durability in PEMFC. This is most likely related to the intrinsic nature of the catalyst supports. A number of novel carbon materials, including 1D carbon nanotubes, 2D graphene, 3D carbon nanocomposites, *etc.*, have recently been investigated for PEMFC due to their promising progress in various aspects such as corrosion resistance and porosity of the material[176-180]. However, the small number of nucleation sites, low charge transfer for the deposition of metal NPs with carbon supports, and the mass transfer between metal and support have been major challenges for device performance. A series of noncarbon-based support based on their inherent properties (as shown in Figure 9D) are able to generate SMSI effect with Pt NPs, which greatly helps to suppress the agglomeration/separation of the metal and promote high performance and durability for PEMFC. Despite progress, there are still gaps and challenges between the properties and practical application of Pt-based catalysts supported by TMOs, primarily due to the poor conductivity of the TMOs supported. TMNs and TMCs, in particular TiN, TiC, and $Mo_xC$, stand out from other materials as Pt NPs support in terms of the ORR activity and stability in half-cell tests and the performance and durability in fuel cells with reported values well above those of carbon-supported Pt-based catalysts.

## PERSPECTIVE AND OUTLOOK

The development of high-stability carbon-free Pt-based catalysts is scientifically and technically essential to facilitate their practical application in fuel cells. As discussed in this review, a series of TMOs-, TMNs-, and TMCs-supported Pt-based catalysts provide an excellent opportunity to substitute the use of carbon at the cathode for PEMFCs. Innovative and effective construct strategies of SMSI are essential to improve the

catalytic activity and stability with regards to improving the electron conduction, suppressing the chemisorption of small molecules, and increasing the interaction between metal and support. However, a series of significant challenges remain for the application of TM-supported Pt-based catalysts in PEMFCs.

Firstly, metal-oxide systems and metal-carbide systems suffer from several drawbacks, such as low electronic conductivity and limited surface area, which can be efficiently optimized by doping strategies (introducing $V_o$) and coupling superior conductive materials. The SMSI effect between metal and supports can also further be enhanced by doping strategies to change the electronic structure of the support. Metal-nitride systems can effectively avoid these drawbacks due to their high conductivity, while the specific areas of TMNs are generally extremely low due to the fact that the high-temperature annealing process is always needed to synthesize TMNs. In addition, the specific preparation method of the catalysts and the size of the metal NPs can significantly affect the charge transfer between the metal and the support, while the charge transfer between the support and the noble metal particle sizes has rarely been reported. Furthermore, the study of the surface/interface structure and dynamic evolution of TM-supported Pt catalysts in the reaction environment at the atomic scale is important for the rational design of catalysts and revealing the reaction mechanism, whereas the key issues such as the interfacial structure performance relationship in the TM-supported Pt catalytic reaction have not been fully elucidated. Finally, although some typical catalysts with SMSI show considerable activity and durability for ORR in the rotating ring disk electrode level, while few electrocatalysts have not yet been practically promoted and applied to the membrane electrode assembly, thus the practical potential of these catalysts cannot be verified. All in all, although many challenges are still in the way, the SMSI provides great potential to improve the performance of the catalysts for ORR and beyond, shedding light on the practical application of these novel materials with high activity and durability.

## DECLARATION

### Authors' contributions
Conceived and designed the manuscript: Chen M, Miao Z, Tian X
Drafted and revised the manuscript: Chen M, Rao P, Miao Z, Luo J, Li J, Deng P, Huang W, Tian X

### Availability of data and materials
Not applicable.

### Conflicts of interest
All authors declared that there are no conflicts of interest.

### Ethical approval
Not applicable.

### Consent to participate
Not applicable.

**Copyright**

## REFERENCES

1.   Li C, Tan H, Lin J, et al. Emerging Pt-based electrocatalysts with highly open nanoarchitectures for boosting oxygen reduction reaction. *Nano Today* 2018;21:91-105.  DOI

2.   Chalgin A, Song C, Tao P, Shang W, Deng T, Wu J. Effect of supporting materials on the electrocatalytic activity, stability and selectivity of noble metal-based catalysts for oxygen reduction and hydrogen evolution reactions. *Prog Nat Sci Mater* 2020;30:289-97.  DOI

3.   Wu G, More KL, Johnston CM, Zelenay P. High-performance electrocatalysts for oxygen reduction derived from polyaniline, iron, and cobalt. *Science* 2011;332:443-7.  DOI  PubMed

4.   Kodama K, Nagai T, Kuwaki A, Jinnouchi R, Morimoto Y. Challenges in applying highly active Pt-based nanostructured catalysts for oxygen reduction reactions to fuel cell vehicles. *Nat Nanotechnol* 2021;16:140-7.  DOI  PubMed

5.   Liu M, Zhao Z, Duan X, Huang Y. Nanoscale structure design for high-performance Pt-based ORR catalysts. *Adv Mater* 2019;31:e1802234.  DOI  PubMed

6.   Miao Z, Wang X, Zhao Z, et al. Improving the stability of non-noble-metal M-N-C catalysts for proton-exchange-membrane fuel cells through M-N bond length and coordination regulation. *Adv Mater* 2021;33:e2006613.  DOI

7.   Li S, Hao X, Abudula A, Guan G. Nanostructured Co-based bifunctional electrocatalysts for energy conversion and storage: current status and perspectives. *J Mater Chem A* 2019;7:18674-707.  DOI

8.   He Y, Liu S, Priest C, Shi Q, Wu G. Atomically dispersed metal-nitrogen-carbon catalysts for fuel cells: advances in catalyst design, electrode performance, and durability improvement. *Chem Soc Rev* 2020;49:3484-524.  DOI

9.   Wu Z, Zhang H, Chen C, Li G, Han Y. Applications of in situ electron microscopy in oxygen electrocatalysis. *Microstructures* 2022;2:2022002.  DOI

10.  Frey H, Beck A, Huang X, van Bokhoven JA, Willinger MG. Dynamic interplay between metal nanoparticles and oxide support under redox conditions. *Science* 2022;376:982-7.  DOI  PubMed

11.  Zhang W, Chang J, Wang G, et al. Surface oxygenation induced strong interaction between Pd catalyst and functional support for zinc-air batteries. *Energy Environ Sci* 2022;15:1573-84.  DOI

12.  Miao Z, Li S, Priest C, Wang T, Wu G, Li Q. Effective approaches for designing stable M-N$_x$/C oxygen-reduction catalysts for proton-exchange-membrane fuel cells. *Adv Mater* 2022;34:e2200595.  DOI

13.  Cheng N, Norouzi Banis M, Liu J, et al. Atomic scale enhancement of metal-support interactions between Pt and ZrC for highly stable electrocatalysts. *Energy Environ Sci* 2015;8:1450-5.  DOI

14.  Yang Y, Wu D, Li R, et al. Engineering the strong metal support interaction of titanium nitride and ruthenium nanorods for effective hydrogen evolution reaction. *Appl Catal B Environ* 2022;317:121796.  DOI

15.  Yan D, Chen J, Jia H. Temperature-induced structure reconstruction to prepare a thermally stable single-atom platinum catalyst. *Angew Chem Int Ed* 2020;59:13562-7.  DOI

16.  Yang H, Lu N, Zhang J, et al. Ultra-low single-atom Pt on g-C$_3$N$_4$ for electrochemical hydrogen peroxide production. *Carbon Energy* 2023;2:1-12.  DOI

17.  Ling L, Liu W, Chen S, Hu X, Jiang H. MOF templated nitrogen doped carbon stabilized Pt-Co bimetallic nanoparticles: low Pt content and robust activity toward electrocatalytic oxygen reduction reaction. *ACS Appl Nano Mater* 2018;1:3331-8.  DOI

18.  Zhou M, Liu M, Miao Q, Shui H, Xu Q. Synergetic Pt atoms and nanoparticles anchored in standing carbon-derived from covalent organic frameworks for catalyzing ORR. *Adv Mater Interfaces* 2022;9:2201263.  DOI

19.  Zhai L, Yang S, Yang X, et al. Conjugated covalent organic frameworks as platinum nanoparticle supports for catalyzing the oxygen reduction reaction. *Chem Mater* 2020;32:9747-52.  DOI

20.  Yu X, Guo J, Li B, et al. Sub-nanometer Pt clusters on defective NiFe LDH nanosheets as trifunctional electrocatalysts for water splitting and rechargeable hybrid sodium-air batteries. *ACS Appl Mater Interfaces* 2021;13:26891-903.  DOI

21.  Rao P, Deng Y, Fan W, et al. Movable type printing method to synthesize high-entropy single-atom catalysts. *Nat Commun* 2022;13:5071.  DOI  PubMed  PMC

22.  Chang F, Xiao M, Miao R, et al. Copper-Based catalysts for electrochemical carbon dioxide reduction to multicarbon products. *Electrochem Energy Rev* 2022;5:139-74.  DOI

23.  Wu D, Baaziz W, Gu B, et al. Surface molecular imprinting over supported metal catalysts for size-dependent selective hydrogenation reactions. *Nat Catal* 2021;4:595-606.  DOI

24.  Deelen TW, Hernández Mejía C, de Jong KP. Control of metal-support interactions in heterogeneous catalysts to enhance activity and selectivity. *Nat Catal* 2019;2:955-70.  DOI

25.  Wang H, Wang L, Xiao F. New routes for the construction of strong metal-support interactions. *Sci China Chem* 2022;65:2051-7.  DOI

26.  Luo Z, Zhao G, Pan H, Sun W. Strong metal-support interaction in heterogeneous catalysts. *Adv Energy Mater* 2022;12:2201395.  DOI

27.  Pu T, Zhang W, Zhu M. Engineering heterogeneous catalysis with strong metal-support interactions: characterization, theory and

manipulation. *Angew Chem Int Ed* 2023;62:e202212278.  DOI

28. Li Y, Zhang Y, Qian K, Huang W. Metal-support interactions in metal/oxide catalysts and oxide-metal interactions in oxide/metal inverse catalysts. *ACS Catal* 2022;12:1268-87.  DOI

29. Wu B, Meng H, Morales DM, et al. Nitrogen-rich carbonaceous materials for advanced oxygen electrocatalysis: synthesis, characterization, and activity of nitrogen sites. *Adv Funct Mater* 2022;32:2204137.  DOI

30. Bai J, Yang L, Jin Z, Ge J, Xing W. Advanced Pt-based intermetallic nanocrystals for the oxygen reduction reaction. *Chinese J Catal* 2022;43:1444-58.  DOI

31. Wang J, Kong H, Zhang J, Hao Y, Shao Z, Ciucci F. Carbon-based electrocatalysts for sustainable energy applications. *Prog Mater Sci* 2021;116:100717.  DOI

32. Yang X, Priest C, Hou Y, Wu G. Atomically dispersed dual-metal-site PGM-free electrocatalysts for oxygen reduction reaction: opportunities and challenges. *SusMat* 2022;2:569-90.  DOI

33. Tian X, Lu XF, Xia BY, Lou XW. Advanced electrocatalysts for the oxygen reduction reaction in energy conversion technologies. *Joule* 2020;4:45-68.  DOI

34. Nørskov JK, Rossmeisl J, Logadottir A, et al. Origin of the overpotential for oxygen reduction at a fuel-cell cathode. *J Phys Chem B* 2004;108:17886-92.  DOI

35. Tian X, Zhao X, Su YQ, et al. Engineering bunched Pt-Ni alloy nanocages for efficient oxygen reduction in practical fuel cells. *Science* 2019;366:850-6.  DOI

36. Ando F, Gunji T, Tanabe T, et al. Enhancement of the oxygen reduction reaction activity of Pt by tuning its *d*-band center via transition metal oxide support interactions. *ACS Catal* 2021;11:9317-32.  DOI

37. Tauster SJ, Fung SC, Garten RL. ChemInform abstract: strong metal-support interactions. group 8 noble metals supported on Titanium dioxide. *Chemischer Informationsdienst* 1978;9:170-5.  DOI

38. Tauster S. Strong metal-support interactions: occurrence among the binary oxides of groups IIA-VB. *J Catal* 1978;55:29-35.  DOI

39. Beck A, Huang X, Artiglia L, et al. The dynamics of overlayer formation on catalyst nanoparticles and strong metal-support interaction. *Nat Commun* 2020;11:3220.  DOI  PubMed  PMC

40. Wang X, Beck A, van Bokhoven JA, Palagin D. Thermodynamic insights into strong metal-support interaction of transition metal nanoparticles on titania: simple descriptors for complex chemistry. *J Mater Chem A* 2021;9:4044-54.  DOI

41. Zhao W, Zhou D, Han S, et al. Metal-support interaction in Pt/TiO$_2$: formation of surface Pt-Ti alloy. *J Phys Chem C* 2021;125:10386-96.  DOI

42. Du X, Tang H, Qiao B. Oxidative strong metal-support interactions. *Catalysts* 2021;11:896.  DOI

43. Macino M, Barnes AJ, Althahban SM, et al. Tuning of catalytic sites in Pt/TiO$_2$ catalysts for the chemoselective hydrogenation of 3-nitrostyrene. *Nat Catal* 2019;2:873-81.  DOI

44. Kennedy RM, Crosby LA, Ding K, et al. Replication of SMSI via ALD: TiO$_2$ overcoats increase Pt-catalyzed acrolein hydrogenation selectivity. *Catal Lett* 2018;148:2223-32.  DOI

45. Komanoya T, Kinemura T, Kita Y, Kamata K, Hara M. Electronic effect of ruthenium nanoparticles on efficient reductive amination of carbonyl compounds. *J Am Chem Soc* 2017;139:11493-9.  DOI  PubMed

46. Zhang L, Persaud R, Theodore EM. Ultrathin metal films on a metal oxide surface: growth of Au on TiO$_2$ (110). *Phys Rev B* 1997;56:10549-57.  DOI

47. Gubó R, Yim CM, Allan M, Pang CL, Berkó A, Thornton G. Variation of SMSI with the Au:Pd ratio of bimetallic nanoparticles on TiO$_2$ (110). *Top Catal* 2018;61:308-17.  DOI  PubMed  PMC

48. Fu Q, Wagner T, Olliges S, Carstanjen HD. Metal-oxide interfacial reactions: encapsulation of Pd on TiO$_2$ (110). *J Phys Chem B* 2005;109:944-51.  DOI  PubMed

49. Liu X, Liu MH, Luo YC, et al. Strong metal-support interactions between gold nanoparticles and ZnO nanorods in CO oxidation. *J Am Chem Soc* 2012;134:10251-8.  DOI

50. Tang H, Wei J, Liu F, et al. Strong metal-support interactions between gold nanoparticles and nonoxides. *J Am Chem Soc* 2016;138:56-9.  DOI

51. Tang H, Su Y, Guo Y, et al. Oxidative strong metal-support interactions (OMSI) of supported platinum-group metal catalysts. *Chem Sci* 2018;9:6679-84.  DOI  PubMed  PMC

52. Liu S, Xu W, Niu Y, et al. Ultrastable Au nanoparticles on titania through an encapsulation strategy under oxidative atmosphere. *Nat Commun* 2019;10:5790.  DOI  PubMed  PMC

53. Liu S, Qi H, Zhou J, et al. Encapsulation of platinum by titania under an oxidative atmosphere: contrary to classical strong metal-support interactions. *ACS Catal* 2021;11:6081-90.  DOI

54. Matsubu JC, Zhang S, DeRita L, et al. Adsorbate-mediated strong metal-support interactions in oxide-supported Rh catalysts. *Nat Chem* 2017;9:120-7.  DOI

55. Wang X, Liu Y, Peng X, Lin B, Cao Y, Jiang L. Sacrificial adsorbate strategy achieved strong metal-support interaction of stable Cu nanocatalysts. *ACS Appl Energy Mater* 2018;1:1408-14.  DOI

56. Xin H, Lin L, Li R, et al. Overturning CO$_2$ hydrogenation selectivity with high activity via reaction-induced strong metal-support interactions. *J Am Chem Soc* 2022;144:4874-82.  DOI

57. Li D, Xu F, Tang X, et al. Induced activation of the commercial Cu/ZnO/Al$_2$O$_3$ catalyst for the steam reforming of methanol. *Nat Catal* 2022;5:99-108.  DOI

58. Zhang J, Wang H, Wang L, et al. Wet-chemistry strong metal-support interactions in Titania-supported Au catalysts. *J Am Chem Soc* 2019;141:2975-83.  DOI

59. Hao H, Jin B, Liu W, Wu X, Yin F, Liu S. Robust Pt@TiO$_x$/TiO$_2$ catalysts for hydrocarbon combustion: effects of Pt-TiO$_x$ interaction and sulfates. *ACS Catal* 2020;10:13543-8.  DOI

60. Wang L, Zhang J, Zhu Y, et al. Strong metal-support interactions achieved by hydroxide-to-oxide support transformation for preparation of sinter-resistant gold nanoparticle catalysts. *ACS Catal* 2017;7:7461-5.  DOI

61. Dong J, Fu Q, Jiang Z, Mei B, Bao X. Carbide-supported Au catalysts for water-gas shift reactions: a new territory for the strong metal-support interaction effect. *J Am Chem Soc* 2018;140:13808-16.  DOI  PubMed

62. Dong J, Fu Q, Li H, et al. Reaction-induced strong metal-support interactions between metals and inert boron nitride nanosheets. *J Am Chem Soc* 2020;142:17167-74.  DOI

63. Sato K, Miyahara S, Tsujimaru K, et al. Barium oxide encapsulating cobalt nanoparticles supported on magnesium oxide: active non-noble metal catalysts for ammonia synthesis under mild reaction conditions. *ACS Catal* 2021;11:13050-61.  DOI

64. Wang H, Wang L, Lin D, et al. Strong metal-support interactions on gold nanoparticle catalysts achieved through Le Chatelier's principle. *Nat Catal* 2021;4:418-24.  DOI

65. Chen H, Yang Z, Wang X, et al. Photoinduced strong metal-support interaction for enhanced catalysis. *J Am Chem Soc* 2021;143:8521-6.  DOI

66. Zhang J, Zhu D, Yan J, Wang CA. Strong metal-support interactions induced by an ultrafast laser. *Nat Commun* 2021;12:6665.  DOI  PubMed  PMC

67. Ma Z, Li S, Wu L, et al. NbO$_x$ nano-nail with a Pt head embedded in carbon as a highly active and durable oxygen reduction catalyst. *Nano Energy* 2020;69:104455.  DOI

68. Mirshekari G, Rice C. Effects of support particle size and Pt content on catalytic activity and durability of Pt/TiO$_2$ catalyst for oxygen reduction reaction in proton exchange membrane fuel cells environment. *J Power Sources* 2018;396:606-14.  DOI

69. Shi W, Park A, Xu S, Yoo PJ, Kwon Y. Continuous and conformal thin TiO$_2$-coating on carbon support makes Pd nanoparticles highly efficient and durable electrocatalyst. *Appl Catal B Environ* 2021;284:119715.  DOI

70. Deng X, Yin S, Wu X, Sun M, Xie Z, Huang Q. Synthesis of PtAu/TiO$_2$ nanowires with carbon skin as highly active and highly stable electrocatalyst for oxygen reduction reaction. *Electrochim Acta* 2018;283:987-96.  DOI

71. Mirshekari G, Shirvanian A. A comparative study on catalytic activity and stability of TiO$_2$, TiN, and TiC supported Pt electrocatalysts for oxygen reduction reaction in proton exchange membrane fuel cells environment. *J Electroanal Chem* 2019;840:391-9.  DOI

72. Wang J, Xu M, Zhao J, et al. Anchoring ultrafine Pt electrocatalysts on TiO$_2$-C via photochemical strategy to enhance the stability and efficiency for oxygen reduction reaction. *Appl Catal B Environ* 2018;237:228-36.  DOI

73. Shi W, Park A, Li Z, et al. Sub-nanometer thin TiO$_2$-coating on carbon support for boosting oxygen reduction activity and durability of Pt nanoparticles. *Electrochim Acta* 2021;394:139127.  DOI

74. Li J, Zhou H, Zhuo H, et al. Oxygen vacancies on TiO$_2$ promoted the activity and stability of supported Pd nanoparticles for the oxygen reduction reaction. *J Mater Chem A* 2018;6:2264-72.  DOI

75. Chen Y, Chen J, Zhang J, Xue Y, Wang G, Wang R. Anchoring highly dispersed Pt electrocatalysts on TiO$_x$ with strong metal-support interactions via an oxygen vacancy-assisted strategy as durable catalysts for the oxygen reduction reaction. *Inorg Chem* 2022;61:5148-56.  DOI

76. Huynh TT, Pham HQ, Nguyen AV, Nguyen ST, Bach LG, Ho VTT. High conductivity and surface area of mesoporous Ti$_{0.7}$W$_{0.3}$O$_2$ materials as promising catalyst support for Pt in proton-exchange membrane fuel cells. *J Nanosci Nanotechnol* 2019;19:877-81.  DOI

77. Subban CV, Zhou Q, Hu A, Moylan TE, Wagner FT, DiSalvo FJ. Sol-Gel synthesis, electrochemical characterization, and stability testing of Ti$_{0.7}$W$_{0.3}$O$_2$ nanoparticles for catalyst support applications in proton-exchange membrane fuel cells. *J Am Chem Soc* 2010;132:17531-6.  DOI

78. Hsieh B, Tsai M, Pan C, et al. Platinum loaded on dual-doped TiO$_2$ as an active and durable oxygen reduction reaction catalyst. *NPG Asia Mater* 2017;9:e403-e403.  DOI

79. Shahgaldi S, Hamelin J. The effect of low platinum loading on the efficiency of PEMFC's electrocatalysts supported on TiO$_2$-Nb, and SnO$_2$-Nb: an experimental comparison between active and stable conditions. *Energy Convers Manag* 2015;103:681-90.  DOI

80. Wang Y, Wilkinson DP, Guest A, et al. Synthesis of Pd and Nb-doped TiO$_2$ composite supports and their corresponding Pt-Pd alloy catalysts by a two-step procedure for the oxygen reduction reaction. *J Power Sources* 2013;221:232-41.  DOI

81. Senevirathne K, Neburchilov V, Alzate V, et al. Nb-doped TiO$_2$/carbon composite supports synthesized by ultrasonic spray pyrolysis for proton exchange membrane (PEM) fuel cell catalysts. *J Power Sources* 2012;220:1-9.  DOI

82. Bing Y, Neburchilov V, Song C, et al. Effects of synthesis condition on formation of desired crystal structures of doped-TiO$_2$/carbon composite supports for ORR electrocatalysts. *Electrochim Acta* 2012;77:225-31.  DOI

83. Huang S, Ganesan P, Popov BN. Electrocatalytic activity and stability of niobium-doped titanium oxide supported platinum catalyst for polymer electrolyte membrane fuel cells. *Appl Catal B Environ* 2010;96:224-31.  DOI

84. Noh K, Nam I, Han JW. Nb-TiO$_2$ nanotubes as catalyst supports with high activity and durability for oxygen reduction. *Appl Surf Sci* 2020;521:146330.  DOI

85. Kim J, Kwon G, Lim H, Zhu C, You H, Kim Y. Effects of transition metal doping in Pt/M-TiO$_2$ (M = V, Cr, and Nb) on oxygen reduction reaction activity. *J Power Sources* 2016;320:188-95.  DOI

86.     Kim J, Chang S, Kim Y. Compressive strain as the main origin of enhanced oxygen reduction reaction activity for Pt electrocatalysts on chromium-doped titania support. *Appl Catal B Environ* 2014;158-159:112-8.  DOI

87.     Ho VT, Pan CJ, Rick J, Su WN, Hwang BJ. Nanostructured $Ti_{0.7}Mo_{0.3}O_2$ support enhances electron transfer to Pt: high-performance catalyst for oxygen reduction reaction. *J Am Chem Soc* 2011;133:11716-24.  DOI

88.     Tsai M, Nguyen T, Akalework NG, et al. Interplay between molybdenum dopant and oxygen vacancies in a $TiO_2$ support enhances the oxygen reduction reaction. *ACS Catal* 2016;6:6551-9.  DOI

89.     Kumar A, Ramani V. Strong metal-support interactions enhance the activity and durability of platinum supported on tantalum-modified titanium dioxide electrocatalysts. *ACS Catal* 2014;4:1516-25.  DOI

90.     Stassi A, Gatto I, Baglio V, Passalacqua E, Aricò AS. Oxide-supported PtCo alloy catalyst for intermediate temperature polymer electrolyte fuel cells. *Appl Catal B Environ* 2013;142-143:15-24.  DOI

91.     Noh K, Im H, Lim C, Jang MG, Nam I, Han JW. Tunable nano-distribution of Pt on $TiO_2$ nanotubes by atomic compression control for high-efficient oxygen reduction reaction. *Chem Eng J* 2022;427:131568.  DOI

92.     Tsai M, Rick J, Su W, Hwang B. Design of transition-metal-doped $TiO_2$ as a multipurpose support for fuel cell applications: using a computational high-throughput material screening approach. *Mol Syst Des Eng* 2017;2:449-56.  DOI

93.     Murphin Kumar PS, Ponnusamy VK, Deepthi KR, et al. Controlled synthesis of Pt nanoparticle supported $TiO_2$ nanorods as efficient and stable electrocatalysts for the oxygen reduction reaction. *J Mater Chem A* 2018;6:23435-44.  DOI

94.     Masuda T, Fukumitsu H, Fugane K, et al. Role of cerium oxide in the enhancement of activity for the oxygen reduction reaction at Pt-$CeO_x$ nanocomposite electrocatalyst - an in situ electrochemical X-ray absorption fine structure study. *J Phys Chem C* 2012;116:10098-102.  DOI

95.     Chen J, Li Z, Chen Y, et al. An enhanced activity of Pt/$CeO_2$/CNT triple junction interface catalyst prepared by atomic layer deposition for oxygen reduction reaction. *Chem Phys Lett* 2020;755:137793.  DOI

96.     Du C, Gao X, Cheng C, Zhuang Z, Li X, Chen W. Metal organic framework for the fabrication of mutually interacted Pt $CeO_2$C ternary nanostructure: advanced electrocatalyst for oxygen reduction reaction. *Electrochim Acta* 2018;266:348-56.  DOI

97.     Xu F, Wang D, Sa B, Yu Y, Mu S. One-pot synthesis of Pt/$CeO_2$/C catalyst for improving the ORR activity and durability of PEMFC. *Int J Hydrog Energy* 2017;42:13011-9.  DOI

98.     Tan N, Lei Y, Huo D, et al. Fabricating Pt/$CeO_2$/N-C ternary ORR electrocatalysts with extremely low platinum content and excellent performance. *J Mater Sci* 2022;57:538-52.  DOI

99.     Lu Q, Wang Z, Tang Y, et al. Well-controlled Pt-$CeO_2$-nitrogen doped carbon triple-junction catalysts with enhanced activity and durability for the oxygen reduction reaction. *Sustain Energy Fuels* 2022;6:2989-95.  DOI

100.    Kim GY, Yoon KR, Shin K, Jung JW, Henkelman G, Ryu WH. Black tungsten oxide nanofiber as a robust support for metal catalysts: high catalyst loading for electrochemical oxygen reduction. *Small* 2021;17:e2103755.  DOI

101.    Kumar S, Bhange SN, Soni R, Kurungot S. $WO_3$ nanorods bearing interconnected Pt nanoparticle units as an activity-modulated and corrosion-resistant carbon-free system for polymer electrolyte membrane fuel cells. *ACS Appl Energy Mater* 2020;3:1908-21.  DOI

102.    Jin Y. $WO_3$ modified graphene supported Pt electrocatalysts with enhanced performance for oxygen reduction reaction. *Int J Electrochem Sci* 2017;12:6535-44.  DOI

103.    Mo Y, Feng S, Yu T, et al. Surface unsaturated $WO_x$ activating PtNi alloy nanowires for oxygen reduction reaction. *J Colloid Interface Sci* 2022;607:1928-35.  DOI

104.    Lee J, Yim D, Park JH, et al. Tuning *d*-band centers by coupling PdO nanoclusters to $WO_3$ nanosheets to promote the oxygen reduction reaction. *J Mater Chem A* 2020;8:13490-500.  DOI

105.    Song Z, Banis MN, Zhang L, et al. Origin of achieving the enhanced activity and stability of Pt electrocatalysts with strong metal-support interactions via atomic layer deposition. *Nano Energy* 2018;53:716-25.  DOI

106.    Gao W, Zhang Z, Dou M, Wang F. Highly dispersed and crystalline $Ta_2O_5$ anchored Pt electrocatalyst with improved activity and durability toward oxygen reduction: promotion by atomic-scale Pt-$Ta_2O_5$ interactions. *ACS Catal* 2019;9:3278-88.  DOI

107.    Hung Y, Liu W, Chen Y, Wang K, Perng T. On the mesoporous TiN catalyst support for proton exchange membrane fuel cell. *Int J Hydrog Energy* 2020;45:14083-92.  DOI

108.    Tian X, Luo J, Nan H, Fu Z, Zeng J, Liao S. Binary transition metal nitrides with enhanced activity and durability for the oxygen reduction reaction. *J Mater Chem A* 2015;3:16801-9.  DOI

109.    Tian X, Luo J, Nan H, et al. Transition metal nitride coated with atomic layers of Pt as a low-cost, highly stable electrocatalyst for the oxygen reduction reaction. *J Am Chem Soc* 2016;138:1575-83.  DOI

110.    Shin H, Kim H, Chung DY, et al. Scaffold-like titanium nitride nanotubes with a highly conductive porous architecture as a nanoparticle catalyst support for oxygen reduction. *ACS Catal* 2016;6:3914-20.  DOI

111.    Pan Z, Xiao Y, Fu Z, et al. Hollow and porous titanium nitride nanotubes as high-performance catalyst supports for oxygen reduction reaction. *J Mater Chem A* 2014;2:13966.  DOI

112.    Xiao Y, Zhan G, Fu Z, et al. Robust non-carbon titanium nitride nanotubes supported Pt catalyst with enhanced catalytic activity and durability for methanol oxidation reaction. *Electrochim Acta* 2014;141:279-85.  DOI

113.    Chen X, Li W, Pan Z, et al. Non-carbon titanium cobalt nitride nanotubes supported platinum catalyst with high activity and durability for methanol oxidation reaction. *Appl Surf Sci* 2018;440:193-201.  DOI

114.    Chen X, Pan Z, Zhou Q, et al. Pt nanoparticles supported on non-carbon titanium chromium nitride nanotubes with high activity and durability for methanol oxidation reaction. *J Solid State Electrochem* 2019;23:315-24.  DOI

115.    Wu Z, Dang D, Tian X. Designing robust support for Pt alloy nanoframes with durable oxygen reduction reaction activity. *ACS Appl Mater Interfaces* 2019;11:9117-24.  DOI  PubMed

116.    Yu F, Xie Y, Tang H, et al. Platinum decorated hierarchical porous structures composed of ultrathin titanium nitride nanoflakes for efficient methanol oxidation reaction. *Electrochim Acta* 2018;264:216-24.  DOI

117.    Zheng Y, Zhang J, Zhan H, Sun D, Dang D, Tian XL. Porous and three dimensional titanium nitride supported platinum as an electrocatalyst for oxygen reduction reaction. *Electrochem Commun* 2018;91:31-5.  DOI

118.    Feng G, Pan Z, Xu Y, et al. Platinum decorated mesoporous titanium cobalt nitride nanorods catalyst with promising activity and CO-tolerance for methanol oxidation reaction. *Int J Hydrog Energy* 2018;43:17064-8.  DOI

119.    Yuan Z, Cao Y, Zhang Z, et al. Dandelion-like titanium nitride supported platinum as an efficient oxygen reduction catalyst in acidic media. *Int J Hydrog Energy* 2022;47:15035-43.  DOI

120.    Yang M, Van Wassen AR, Guarecuco R, Abruña HD, DiSalvo FJ. Nano-structured ternary niobium titanium nitrides as durable non-carbon supports for oxygen reduction reaction. *Chem Commun* 2013;49:10853-5.  DOI  PubMed

121.    Xiao Y, Fu Z, Zhan G, et al. Increasing Pt methanol oxidation reaction activity and durability with a titanium molybdenum nitride catalyst support. *J Power Sources* 2015;273:33-40.  DOI

122.    Tian X, Tang H, Luo J, Nan H, Shu T. High-performance core-shell catalyst with nitride nanoparticles as a core: well-defined titanium copper nitride coated with an atomic Pt layer for the oxygen reduction reaction. *ACS Catal* 2017;7:3810-7.  DOI

123.    Liu Q, Du L, Fu G, et al. Structurally ordered Fe$_3$Pt nanoparticles on robust nitride support as a high performance catalyst for the oxygen reduction reaction. *Adv Energy Mater* 2019;9:1803040.  DOI

124.    Nan H, Dang D, Tian XL. Structural engineering of robust titanium nitride as effective platinum support for the oxygen reduction reaction. *J Mater Chem A* 2018;6:6065-73.  DOI

125.    Yin J, Wang L, Tian C, et al. Low-Pt loaded on a vanadium nitride/graphitic carbon composite as an efficient electrocatalyst for the oxygen reduction reaction. *Chemistry* 2013;19:13979-86.  DOI

126.    Kim NY, Lee JH, Kwon JA, et al. Vanadium nitride nanofiber membrane as a highly stable support for Pt-catalyzed oxygen reduction reaction. *J Ind Eng Chem* 2017;46:298-303.  DOI

127.    Zheng J, Zhang W, Zhang J, et al. Recent advances in nanostructured transition metal nitrides for fuel cells. *J Mater Chem A* 2020;8:20803-18.  DOI

128.    Yang M, Cui Z, DiSalvo FJ. Mesoporous chromium nitride as a high performance non-carbon support for the oxygen reduction reaction. *Phys Chem Chem Phys* 2013;15:7041-4.  DOI  PubMed

129.    Yang M, Guarecuco R, Disalvo FJ. Mesoporous chromium nitride as high performance catalyst support for methanol electrooxidation. *Chem Mater* 2013;25:1783-7.  DOI

130.    Liu B, Huo L, Si R, Liu J, Zhang J. A general method for constructing two-dimensional layered mesoporous mono- and binary-transition-metal nitride/graphene as an ultra-efficient support to enhance its catalytic activity and durability for electrocatalytic application. *ACS Appl Mater Interfaces* 2016;8:18770-87.  DOI

131.    Chemler SR, Bovino MT. Catalytic aminohalogenation of alkenes and alkynes. *ACS Catal* 2013;3:1076-91.  DOI

132.    He C, Tao J. Transition metal carbides coupled with nitrogen-doped carbon as efficient and stable Bi-functional catalysts for oxygen reduction reaction and hydrogen evolution reaction. *Int J Hydrog Energy* 2022;47:13240-50.  DOI

133.    Hunt ST, Milina M, Alba-Rubio AC, et al. Self-assembly of noble metal monolayers on transition metal carbide nanoparticle catalysts. *Science* 2016;352:974-8.  DOI

134.    Yue R, Xia M, Wang M, et al. TiN and TiC as stable and promising supports for oxygen reduction reaction: theoretical and experimental study. *Appl Surf Sci* 2019;495:143620.  DOI

135.    Lee Y, Ahn JH, Park H, et al. Support structure-catalyst electroactivity relation for oxygen reduction reaction on platinum supported by two-dimensional titanium carbide. *Nano Energy* 2021;79:105363.  DOI

136.    Xie X, Chen S, Ding W, Nie Y, Wei Z. An extraordinarily stable catalyst: Pt NPs supported on two-dimensional Ti$_3$C$_2$X$_2$ (X = OH, F) nanosheets for oxygen reduction reaction. *Chem Commun* 2013;49:10112-4.  DOI

137.    Ignaszak A, Song C, Zhu W, et al. Titanium carbide and its core-shelled derivative TiC@TiO$_2$ as catalyst supports for proton exchange membrane fuel cells. *Electrochim Acta* 2012;69:397-405.  DOI

138.    Xie X, Xue Y, Li L, et al. Surface Al leached Ti$_3$AlC$_2$ as a substitute for carbon for use as a catalyst support in a harsh corrosive electrochemical system. *Nanoscale* 2014;6:11035-40.  DOI

139.    Min P, Li C, Ding L, Jian Z, Liang C. Microwave-assisted preparation of Mo$_2$C/CNTs nanocomposites as efficient electrocatalyst supports for oxygen reduction reaction. *Ind Eng Chem Res* 2010;175:275-8.  DOI

140.    Cheng C, Zhang X, Fu Z, Yang Z. Strong metal-support interactions impart activity in the oxygen reduction reaction: Au monolayer on Mo$_2$C (MXene). *J Phys Condens Matter* 2018;30:475201.  DOI

141.    Saha S, Cabrera Rodas JA, Tan S, Li D. Performance evaluation of platinum-molybdenum carbide nanocatalysts with ultralow platinum loading on anode and cathode catalyst layers of proton exchange membrane fuel cells. *J Power Sources* 2018;378:742-9.  DOI

142.    Hamo ER, Rosen BA. Improved durability and activity in Pt/Mo$_2$C fuel cell cathodes by magnetron sputtering of tantalum. *ChemElectroChem* 2021;8:3123-34.  DOI

143.    Elbaz L, Phillips J, Artyushkova K, More K, Brosha EL. Evidence of high electrocatalytic activity of molybdenum carbide supported platinum nanorafts. *J Electrochem Soc* 2015;162:H681-5.  DOI

144. Krishnamurthy CB, Lori O, Elbaz L, Grinberg I. First-principles investigation of the formation of Pt nanorafts on a $Mo_2C$ support and their catalytic activity for oxygen reduction reaction. *J Phys Chem Lett* 2018;9:2229-34.  DOI  PubMed

145. Schweitzer NM, Schaidle JA, Ezekoye OK, Pan X, Linic S, Thompson LT. High activity carbide supported catalysts for water gas shift. *J Am Chem Soc* 2011;133:2378-81.  DOI  PubMed

146. Zhang K, Yang W, Ma C, et al. A highly active, stable and synergistic Pt nanoparticles/$Mo_2C$ nanotube catalyst for methanol electro-oxidation. *NPG Asia Mater* 2015;7:e153-e153.  DOI

147. Li Q, Ma Z, Sa R, et al. Computation-predicted, stable, and inexpensive single-atom nanocatalyst Pt@$Mo_2C$-an important advanced material for $H_2$ production. *J Mater Chem A* 2017;5:14658-72.  DOI

148. Huang X, Wang J, Gao J, Zhang Z, Gan LY, Xu H. Structural evolution and underlying mechanism of single-atom centers on $Mo_2C$ (100) support during oxygen reduction reaction. *ACS Appl Mater Interfaces* 2021;13:17075-84.  DOI  PubMed

149. Zhang L, Yang T, Zang W, et al. Quasi-paired Pt atomic sites on $Mo_2C$ promoting selective four-electron oxygen reduction. *Adv Sci* 2021;8:e2101344.  DOI  PubMed  PMC

150. Gao W, Liu T, Zhang Z, Dou M, Wang F. Stabilization of Pt nanoparticles at the $Ta_2O_5$-TaC binary junction: an effective strategy to achieve high durability for oxygen reduction. *J Mater Chem A* 2020;8:5525-34.  DOI

151. Begum M, Yurukcu M, Yurtsever F, et al. Pt-Ni/WC alloy nanorods arrays as ORR catalyst for PEM fuel cells. *ECS Trans* 2017;80:919-25.  DOI

152. Yurtsever FM, Yurukcu M, Begum M, Watanabe F, Karabacak T. Stacked and core-shell Pt:Ni/WC nanorod array electrocatalyst for enhanced oxygen reduction reaction in polymer electrolyte membrane fuel cells. *ACS Appl Energy Mater* 2018;1:6115-22.  DOI

153. Nabil Y, Cavaliere S, Harkness I, Sharman J, Jones D, Rozière J. Novel niobium carbide/carbon porous nanotube electrocatalyst supports for proton exchange membrane fuel cell cathodes. *J Power Sources* 2017;363:20-6.  DOI

154. Stamatin SN, Skou EM. Pt/NbC-N electrocatalyst for use in proton exchange membrane fuel cells. *ECS Trans* 2013;58:1267-76.  DOI

155. Justin P, Charan PHK, Rao GR. Activated zirconium carbide promoted Pt/C electrocatalyst for oxygen reduction. *Appl Catal B Environ* 2014;144:767-74.  DOI

156. Hamo ER, Rosen BA. Transition metal carbides as cathode supports for PEM fuel cells. *Nano Res* 2022;15:10218-33.  DOI

157. Wang Y, Wang M, Lu Z, Ma D, Jia Y. Enabling multifunctional electrocatalysts by modifying the basal plane of unifunctional 1T'-$MoS_2$ with anchored transition metal single atoms. *Nanoscale* 2021;13:13390-400.  DOI

158. Logeshwaran N, Panneerselvam IR, Ramakrishnan S, et al. Quasihexagonal platinum nanodendrites decorated over $CoS_2$-N-doped reduced graphene oxide for electro-oxidation of C1-, C2-, and C3-type alcohols. *Adv Sci* 2022;9:e2105344.  DOI  PubMed  PMC

159. Bothra P, Pandey M, Pati SK. Size-selective electrocatalytic activity of $(Pt)_n$/$MoS_2$ for oxygen reduction reaction. *Catal Sci Technol* 2016;6:6389-95.  DOI

160. Anwar MT, Yan X, Asghar MR, et al. $MoS_2$-rGO hybrid architecture as durable support for cathode catalyst in proton exchange membrane fuel cells. *Chinese J Catal* 2019;40:1160-7.  DOI

161. Wei L, Ang EH, Yang Y, et al. Recent advances of transition metal based bifunctional electrocatalysts for rechargeable zinc-air batteries. *J Power Sources* 2020;477:228696.  DOI

162. Wang D, Song Y, Zhang H, Yan X, Guo J. Recent advances in transition metal borides for electrocatalytic oxygen evolution reaction. *J Electroanal Chem* 2020;861:113953.  DOI

163. Cao S, Sun T, Li J, Li Q, Hou C, Sun Q. The cathode catalysts of hydrogen fuel cell: from laboratory toward practical application. *Nano Res* 2023;16:4365-80.  DOI

164. Kumar S, Yoyakki A, Pandikassala A, Soni R, Kurungot S. Pt-anchored-zirconium phosphate nanoplates as high-durable carbon-free oxygen reduction reaction electrocatalyst for PEM fuel cell applications. *Adv Sustain Syst* 2023;7:2200330.  DOI

165. Yin S, Mu S, Lv H, Cheng N, Pan M, Fu Z. A highly stable catalyst for PEM fuel cell based on durable titanium diboride support and polymer stabilization. *Appl Catal B Environ* 2010;93:233-40.  DOI

166. Yin S, Mu S, Pan M, Fu Z. A highly stable $TiB_2$-supported Pt catalyst for polymer electrolyte membrane fuel cells. *J Power Sources* 2011;196:7931-6.  DOI

167. Huang Z, Lin R, Fan R, Fan Q, Ma J. Effect of $TiB_2$ pretreatment on Pt/$TiB_2$ catalyst performance. *Electrochim Acta* 2014;139:48-53.  DOI

168. Zhang C, Ma B, Zhou Y, Wang C. Highly active and durable Pt/MXene nanocatalysts for ORR in both alkaline and acidic conditions. *J Electroanal Chem* 2020;865:114142.  DOI

169. Ponnada S, Kiai MS, Gorle DB, et al. Recent status and challenges in multifunctional electrocatalysis based on 2D MXenes. *Catal Sci Technol* 2022;12:4413-41.  DOI

170. Peera SG, Liu C, Sahu AK, et al. Recent advances on MXene-based electrocatalysts toward oxygen reduction reaction: a focused review. *Adv Mater Interfaces* 2021;8:2100975.  DOI

171. Huang X, Song M, Zhang J, et al. Investigation of MXenes as oxygen reduction electrocatalyst for selective $H_2O_2$ generation. *Nano Res* 2022;15:3927-32.  DOI

172. Xu C, Fan C, Zhang X, et al. MXene ($Ti_3C_2T_x$) and carbon nanotube hybrid-supported platinum catalysts for the high-performance oxygen reduction reaction in PEMFC. *ACS Appl Mater Interfaces* 2020;12:19539-46.  DOI

173. Yang X, Zhang Y, Fu Z, et al. Tailoring the electronic structure of transition metals by the $V_2C$ MXene support: excellent oxygen reduction performance triggered by metal-support interactions. *ACS Appl Mater Interfaces* 2020;12:28206-16.  DOI

174.   Wei B, Fu Z, Legut D, et al. Rational design of highly stable and active MXene-based bifunctional ORR/OER double-atom catalysts. *Adv Mater* 2021;33:e2102595.  DOI

175.   Li Z, Cui Y, Wu Z, et al. Reactive metal-support interactions at moderate temperature in two-dimensional niobium-carbide-supported platinum catalysts. *Nat Catal* 2018;1:349-55.  DOI

176.   Du L, Shao Y, Sun J, Yin G, Liu J, Wang Y. Advanced catalyst supports for PEM fuel cell cathodes. *Nano Energy* 2016;29:314-22. DOI

177.   Samad S, Loh KS, Wong WY, et al. Carbon and non-carbon support materials for platinum-based catalysts in fuel cells. *Int J Hydrog Energy* 2018;43:7823-54.  DOI

178.   Gao Y, Kong D, Liang J, et al. Inside-out dual-doping effects on tubular catalysts: structural and chemical variation for advanced oxygen reduction performance. *Nano Res* 2022;15:361-7.  DOI

179.   Liu X, Zhao Z, Liang J, et al. Inducing covalent atomic interaction in intermetallic Pt alloy nanocatalysts for high-performance fuel cells materials. *Angew Chem Int Ed* 2023;62:e202302134.  DOI

180.   Xiao F, Wang Y, Xu GL, et al. Fe-N-C boosts the stability of supported platinum nanoparticles for fuel cells. *J Am Chem Soc* 2022;144:20372-84.  DOI